genistein were observed in the brain and testis, whereas moderate and high distributions were found in the other hormone target organs (prostate, ovary, and uterus) (Chang et al., 2000). Furthermore, in pregnant rats exposed to genistein, serum genistein concentrations were approximately 5 times less in fetuses than in maternal rats (Doerge et al., 2001). These findings suggest that penetration of genistein into the brain, testis, and fetus are limited by the blood-brain, -testis, and -placental barriers, attenuating the toxicological effects of genistein on the development of the brain, testis, and fetus.

Here we investigated the role of the breast cancer resistance protein (Bcrp/*Abcg2*) in the disposition of phytoestrogens. Bcrp is a member of the ATP-binding cassette transporter family and mediates the efflux transport of endo- and xenobiotics. Bcrp is expressed in various normal tissues (Maliepaard et al., 2001), and cumulative in vivo studies, particularly using *Bcrp*$^{-/-}$ mice, revealed important roles for this protein in the site of absorption and in clearance organs (van Herwaarden et al., 2003; Breedveld et al., 2004; Mizuno et al., 2004; Hirano et al., 2005). In addition, BCRP is also expressed in various tissue barriers, such as those in the brain, testis, and placenta (Jonker et al., 2002; Zhang et al., 2003; Bart et al., 2004). In these tissue barriers, Bcrp is expressed in the plasma membranes facing circulating blood and has its protective role against xenobiotics. Indeed, it was shown using *Bcrp*$^{-/-}$ mice that Bcrp restricts the penetration of imatinib and topotecan into the brain and fetus, respectively (Jonker et al., 2002; Breedveld et al., 2005). As far as phytoestrogens are concerned, many of them can interact with human BCRP at least as inhibitors, but genistein was found to be a BCRP substrate (Imai et al., 2004). Here, we compared the plasma concentration time profiles and tissue distribution of phytoestrogens (daidzein, genistein, and coumestrol) in the brain, testis, epididymis, and fetus using *Bcrp*$^{-/-}$ mice. We found that Bcrp limited the oral availability and penetration into the brain, testis, and epididymis of genistein and the penetration of daidzein and coumestrol into the brain and testis.

Materials and Methods

Materials and Animals

Daidzein, genistein, and coumestrol were purchased from Sigma-Aldrich (St. Louis, MO), and ^{14}C-labeled inulin was from Moravek Biochemicals (Brea, CA). All of the other chemicals were commercially available and of reagent grade. Wild-type FVB mice and *Bcrp*$^{-/-}$ mice (Jonker et al., 2002) were used in the present study. Male mice (9–17 weeks old and 23–32 g body weight) were used in the studies of oral administration and tissue distribution (brain, testis, and epididymis). Female mice (15–16 weeks old and 24–28 g body weight) were used in the ovary distribution study. Pregnant female mice used in the fetus distribution study were at 2 weeks' gestation and weighed 35 to 48 g. All of these animals were maintained under controlled temperature with a light/dark cycle. Food and water were available ad libitum except for the oral administration study in which mice were fasted for approximately 12 h before administration.

Transcellular Transport Study

The transcellular transport study was performed as reported previously with minor modifications (Matsushima et al., 2005). In brief, MDCK II cells were seeded in the 24-well Transwell (Corning, Cambridge, MA) at a density of 1.4×10^5 cells/well and grown for 3 days in Dulbecco's modified Eagle's medium (Invitrogen, Carlsbad, CA) with 10% fetal bovine serum (Sigma-Aldrich) and 1% antibiotic-antimycotic solution (Sigma-Aldrich). The cells were infected with the recombinant adenovirus harboring expression vector for green fluorescent protein (GFP), mouse Bcrp (mBcrp) or human BCRP (hBCRP) at 200 multiplicity of infection. The details of the construction of these recombinant adenoviruses were described in a previous report (Kondo et al., 2004). After 2 days of culture, the cells were used for transport studies. The cells were preincubated in Krebs-Henseleit buffer (142 mM NaCl, 23.8 mM Na_2CO_3, 4.83 mM KCl, 0.96 mM KH_2PO_4, 1.20 mM $MgSO_4$, 12.5 mM HEPES, 5 mM glucose, and 1.53 mM $CaCl_2$, pH 7.4) at 37°C for 30 min, and transport experiments were initiated by replacing the medium on one side of the cell monolayer with Krebs-Henseleit buffer containing 3 μM test compounds. At appropriate times, 100-μl aliquots were taken from the opposite side of the cell monolayer and replaced with 100 μl of buffer.

In vitro transport by mMdr1a was examined using Mdr1a-expressing LLC-PK1 cells (L-Mdr1a). L-Mdr1a was established previously (Smith et al., 1998). L-Mdr1a and parent LLC-PK1 cells were seeded in the 24-well Transwell at a density of 4.8×10^5 cells/well and grown in medium 199 (Invitrogen) with 10% fetal bovine serum and 1% antibiotic-antimycotic solution. Medium was changed on the second day, and cells were subjected to the transport study on the fourth day. The procedures of the transport study were the same as those used for mBcrp and hBCRP. Efflux rates were calculated from the slopes of the time profiles of apical-to-basal and basal-to-apical transport. Flux ratios were obtained by dividing the efflux rates in the basal-to-apical direction by those in the apical-to-basal direction.

Animal Experiments

Oral Administration. Animals were fasted 12 h before administration. Compounds were suspended in 0.5% methylcellulose and orally administered at a dose of 30 μmol/kg. Blood was collected from tail vein at appropriate time points and was centrifuged at 4°C and 1000*g* for 5 min to obtain plasma.

Tissue and Fetus Distribution. Under urethane anesthesia (1.25 g/kg, i.p.), the right jugular vein was cannulated with a polyethylene tube (PE-50; BD Biosciences, San Jose, CA). Compounds were solubilized at a concentration of 1.25 mM in 10% dimethyl sulfoxide/90% saline containing 2 mM NaOH and continuously infused through the cannula at a dose rate of 5 μmol/h/kg. Blood was collected from the left jugular vein at 60, 80, 100, and 120 min and centrifuged at 4°C and 1000*g* for 5 min to obtain plasma. Immediately after the last blood sampling, mice were sacrificed by cervical dislocation, and tissues or fetus was collected. PBS was added to tissues or fetus and homogenized to make 20% homogenate for brain and testis, 10% homogenate for epididymis, 5% homogenate for ovary, and 33% homogenate for fetus. All of the samples were stored at −80°C until use.

[^{14}C]Inulin Distribution. Inulin cannot penetrate cellular membrane, therefore [^{14}C]inulin was used as a marker of space outside of barriers in the brain and testis. Under urethane anesthesia (1.25 g/kg, i.p.), [^{14}C]inulin was administered intravenously from the right jugular vein (50 μCi/kg). At 10-min postdose, blood was collected from the left jugular vein, and mice were sacrificed by cervical dislocation, and then the brain, testis, and epididymis were collected. Blood was centrifuged at 4°C and 1000*g* for 5 min, and plasma was obtained. Plasma (10 μl) was mixed with 8 ml of Hionic-Fluor (PerkinElmer Life and Analytical Sciences, Waltham, MA), and the radioactivity was measured with a liquid scintillation counter (LS 6000SE; Beckman Coulter, Fullerton, CA). Tissues were mixed with 400 μl of hydrogen peroxide and 800 μl of 2-propanol and left for 1 h at room temperature. Subsequently, 1 ml of Soluene 350 (PerkinElmer Life and Analytical Sciences) was added and incubated at 55°C for 4 h to solubilized the tissues. 10 ml of Hionic-Fluor was added and then subjected to a liquid scintillation counter (LS 6000SE).

LC/Mass Spectrometry Analysis

Samples were precipitated with two (for in vitro samples) or three (for in vivo samples) volumes of acetonitrile and centrifuged at 4°C and 15,000*g* for 10 min. After the evaporation of supernatants, the pellets were reconstituted with 10% acetonitrile/90% water and subjected to LC/mass spectrometry analysis. LCMS-2010 EV equipped with a Prominence LC system (Shimadzu, Kyoto, Japan) was used for the analysis. Samples were separated on a CAPCELL PAK C18 MGII column (3 μm, 2 × 50 mm; Shiseido, Tokyo, Japan) in a binary gradient mode. Mobile phase A was 0.05% formic acid, and mobile phase B was acetonitrile. For the analysis of daidzein and genistein, the concentration of mobile phase B was initially 18%, linearly increased up to 60% over 1.5 min, kept at 60% for a further 1 min, and finally re-equilibrated at 18% for 2.5 min. The total run time was 5 min. Daidzein and genistein were eluted at 3.0 and 3.3 min, respectively. For the analysis of coumestrol, the concentration of mobile phase B was initially 25%, linearly increased up to 90% over 1.5 min, kept at 90% for a further 1 min, and finally re-equilibrated at 25% for 3 min. Coumestrol was eluted at 2.7 min. Daidzein, genistein, and coumestrol were detected at mass-to-charge ratios of 255, 269, and 267, respectively, under negative electron-spray ionization mode. The interface voltage was −3.5 kV and the nebulizer gas (N_2) flow was 1.5 l/min. The heat block and curved desolvation line temperatures were 200 and 150°C, respectively.

Quantification of mRNA Level of BCRP in Mouse and Human Epididymis

Mice were anesthetized with ether and sacrificed by exsanguination from the femoral artery and vein. Immediately after sacrifice, the epididymis was collected. Total RNA was isolated from these tissues with using ISOGEN (Wako Pure Chemical Industries, Tokyo, Japan). Total RNA of human epididymis was purchased from BioChain Institute (Hayward, CA). Total RNA from mouse and human epididymis was converted to cDNA using random primer and avian myeloblastosis virus reverse transcriptase. Real-time PCR was performed with a QuantiTect SYBR Green PCR Kit (QIAGEN, Valencia, CA) and a LightCycler system (Roche Diagnostics, Mannheim, Germany). PCR primers were as follows: mouse Bcrp: forward, AAATGGAGCACCTCAACCTG; reverse, CCCATCACAACGTCATCTTG; human BCRP: forward, CAGGTCTGTTGGTCAATCTCACA; reverse, TCCATATCGTGGAATGCTGAAG; mouse GAPDH: forward, ATTGTCAGCAATGCATCCTG; reverse, ATGGACTGTGGTCATGAGCC; and human GAPDH: forward, AATGACCCCTTCATTGAC; reverse, TCCACGACGTACTCAGCGC. External standard curves were generated by dilution of the target PCR product purified by agarose gel electrophoresis. The absolute concentration of the external standard was measured with PicoGreen dsDNA Quantification Reagent (Molecular Probes, Eugene, OR).

Pharmacokinetic Analysis

Area under the curve (AUC) from 0 to 240 min after oral administration was calculated by trapezoidal method. Tissue-to-plasma or fetus-to-plasma concentration ratios (K_p values) were calculated by dividing tissue or fetus concentrations by plasma concentrations at 120-min postdose.

Immunohistochemical Analysis

Frozen sections of the testis and epididymis were prepared from FVB wild-type and *Bcrp*$^{-/-}$ mice and fixed to glass slides in methanol (−20°C). The sections were incubated in 1% Triton X-100 for 30 min at room temperature and subsequently washed with PBS three times. The sections were then incubated in PBS containing 5% bovine serum albumin (BSA-PBS) to block nonspecific protein binding. After washing with PBS three times, the sections were incubated with 1:40 dilution of anti-Bcrp monoclonal antibody (BXP-53; Signet Laboratories, Dedham, MA) in BSA-PBS at 4°C overnight. After washing with PBS three times, the sections were incubated with secondary antibody (Alexa 488 anti-rat IgG; Molecular Probes, Eugene, OR) and Topro3 (Molecular Probes) in BSA-PBS for 1 h at room temperature. The sections were mounted in VECTASHIELD mounting medium (Vector Laboratories, Burlingame, CA).

Statistical Analysis

Statistical analysis for significant differences was performed using the two-tailed Student's *t* test. A probability of <0.05 was considered to be statistically significant.

Results

In Vitro Transport of Phytoestrogens by mBcrp, hBCRP, and Mdr1a. The transport activities of daidzein, genistein, and coumestrol by mBcrp, hBCRP, and mMdr1a were investigated using transporter expressing cell systems (MDCK II/mBcrp, MDCK II/hBCRP, and L-Mdr1a). In those systems, mBcrp, hBCRP, and Mdr1a are localized in the apical membrane and direct the transcellular transport of their substrates in the apical direction (Smith et al., 1998; Matsushima et al., 2005). In MDCK II/mBcrp and MDCK II/hBCRP, the permeability of basal-to-apical direction was greater than that of apical-to-basal direction for all three phytoestrogens, whereas the transcellular transport was almost identical in both directions in MDCK II/GFP (Fig. 1 and Table 1). The flux ratios were higher in MDCK II/mBcrp and MDCK II/hBCRP than those in MDCK II/GFP, suggesting the three phytoestrogens are the substrate of mBcrp and hBCRP. In LLC-PK1 and L-Mdr1a, the permeability of basal-to-apical direction was slightly higher than that of apical-to-basal direction; however, the flux ratios were almost identical between the two cell systems, suggesting the three phytoestrogens are not the substrate of mMdr1a (Fig. 2 and Table 1).

Effects of Bcrp on the In Vivo Disposition of Phytoestrogens. Plasma levels of daidzein, genistein, and coumestrol after oral administration were compared between wild-type and *Bcrp*$^{-/-}$ mice (Fig. 3). Daidzein and genistein exhibited significantly higher plasma exposure in *Bcrp*$^{-/-}$ mice than in wild-type mice (Fig. 3A). The area under the curve over 4 h ($AUC_{0-240\ min}$) was 3.7- and 2.0-fold greater for daidzein and genistein, respectively, than the corresponding control values (Fig. 3B). The plasma exposure of coumestrol was very low compared with the other phytoestrogens, and no significant difference was observed in the $AUC_{0-240\ min}$ of coumestrol between the wild-type and *Bcrp*$^{-/-}$ mice, although significant changes were observed in plasma concentrations at several time points.

Tissue distributions of the phytoestrogens were determined at steady state achieved by a constant intravenous infusion (Fig. 4). Plasma concentrations were almost constant between 60 and 120 min, indicating that plasma concentrations reached a plateau at 60 min (Fig. 4A). The plasma concentrations of daidzein were significantly higher in *Bcrp*$^{-/-}$ mice than that in wild-type mice, but no significant changes were observed for genistein and coumestrol. The K_p values of brain and testis were significantly increased in *Bcrp*$^{-/-}$ mice for all of the three phytoestrogens (Fig. 4B). The fold increases in the K_p values of the brain were 5.6, 9.2, and 3.9 and those in the testis were 5.8, 5.8, and 4.1 for daidzein, genistein, and coumestrol, respectively. The K_p values of [^{14}C]inulin were investigated to estimate the volume of

the capillary space in the brain and testis. The K_p values of [^{14}C]inulin were 0.011 ± 0.004 and 0.031 ± 0.011 (mean ± S.E., n = 3) for the brain and testis, respectively (indicated by a broken line in Fig. 4B). In addition, the effects of Bcrp on the distributions of genistein in the epididymis and ovary were also investigated (Fig. 5). The K_p value of the epididy-

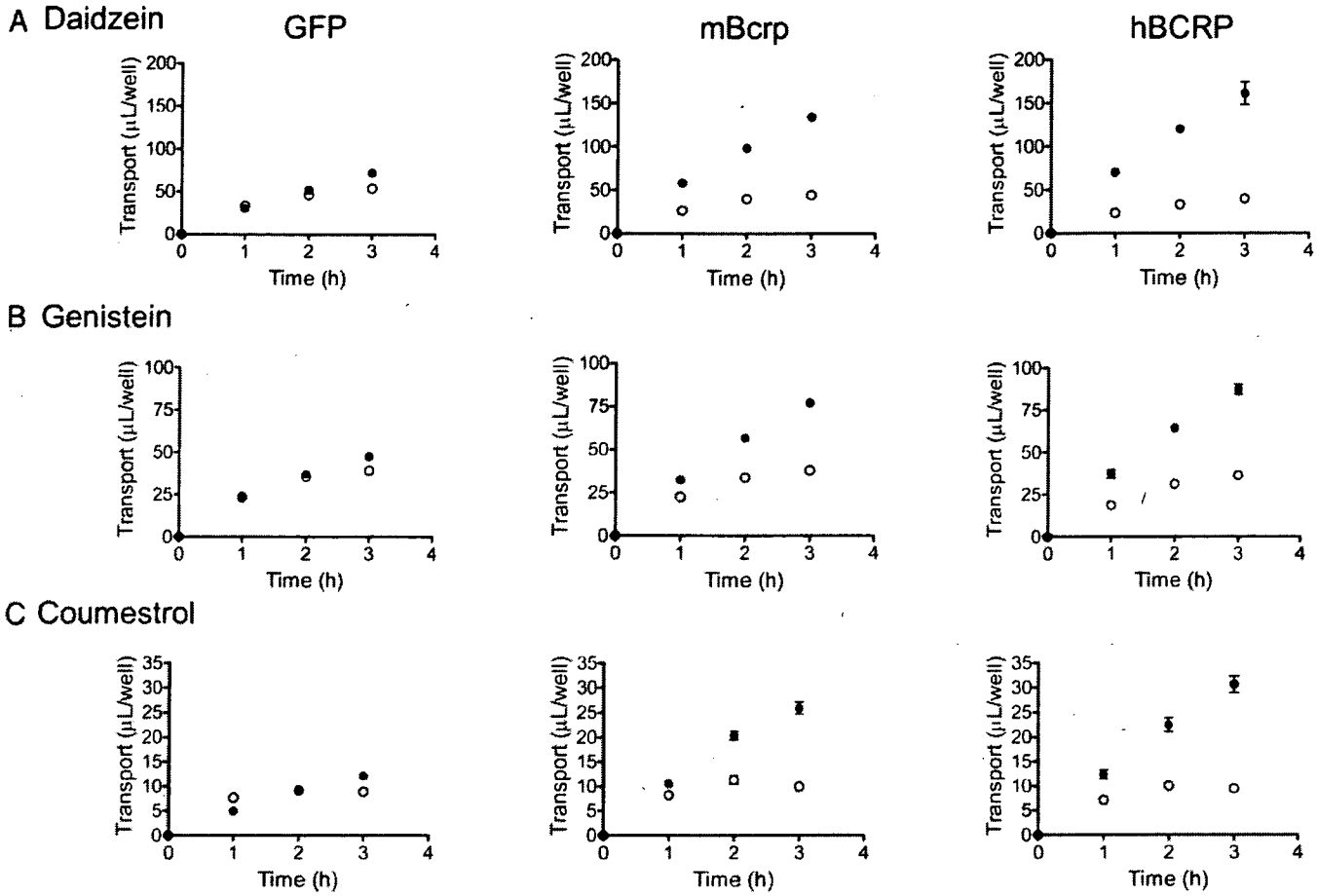

Fig. 1. The transcellular transport of daidzein (A), genistein (B), and coumestrol (C) across monolayers of MDCK II cells expressing the gene for GFP, mBcrp, and hBCRP. Transport in the apical-to-basal direction is represented by ○ and that in the basal-to-apical direction by ●. Data are represented by means ± S.E. of triplicate experiments.

TABLE 1

Transcellular transport of phytoestrogens across MDCK II monolayers expressing mBcrp and hBCRP and across LLC-PK1 monolayer expressing mMdr1a

Data are taken from Figs. 1 and 2. Each value represents the mean ± S.E. A to B represents the permeability of the transcellular transport in the apical to basal direction. B to A represents the permeability of the transcellular transport in the basal to apical direction.

Compound and Cell Line	Permeability		Flux Ratio
	A to B	B to A	
	μl/h/well		
Daidzein			
MDCKII/GFP	17.4 ± 0.2	23.7 ± 0.3	1.36
MDCKII/hBCRP	12.9 ± 0.7	53.2 ± 4.1	4.12
MDCKII/mBcrp	14.7 ± 0.3	44.1 ± 0.8	3.00
LLC-PK1	26.7 ± 1.2	49.9 ± 1.0	1.87
L-Mdr1a	27.9 ± 0.8	47.3 ± 1.0	1.70
Genistein			
MDCKII/GFP	13.0 ± 0.3	15.7 ± 0.4	1.21
MDCKII/hBCRP	12.2 ± 0.8	28.8 ± 1.0	2.36
MDCKII/mBcrp	12.5 ± 0.5	25.6 ± 0.3	2.05
LLC-PK1	54.0 ± 2.3	77.5 ± 0.8	1.44
L-Mdr1a	54.2 ± 1.1	76.0 ± 1.8	1.40
Coumestrol			
MDCKII/GFP	2.80 ± 0.04	4.08 ± 0.18	1.40
MDCKII/hBCRP	3.13 ± 0.15	10.2 ± 0.6	3.26
MDCKII/mBcrp	3.29 ± 0.23	8.75 ± 0.41	2.66
LLC-PK1	11.3 ± 0.4	18.7 ± 0.4	1.65
L-Mdr1a	18.9 ± 0.5	30.9 ± 0.6	1.63

mis was increased in *Bcrp*$^{-/-}$ mice with a fold increase of 2.5, whereas the K_p value of the ovary was unchanged.

Localization of Bcrp in Mouse Testis and Epididymis, and mRNA Expression of *BCRP* in the Human Epididymis. Immunohistochemical analysis was performed to identify the membrane localization of Bcrp protein in the testis and epididymis using the anti-Bcrp antibody (BXP-53) (Fig. 6). In the testis of wild-type mice, Bcrp was detected

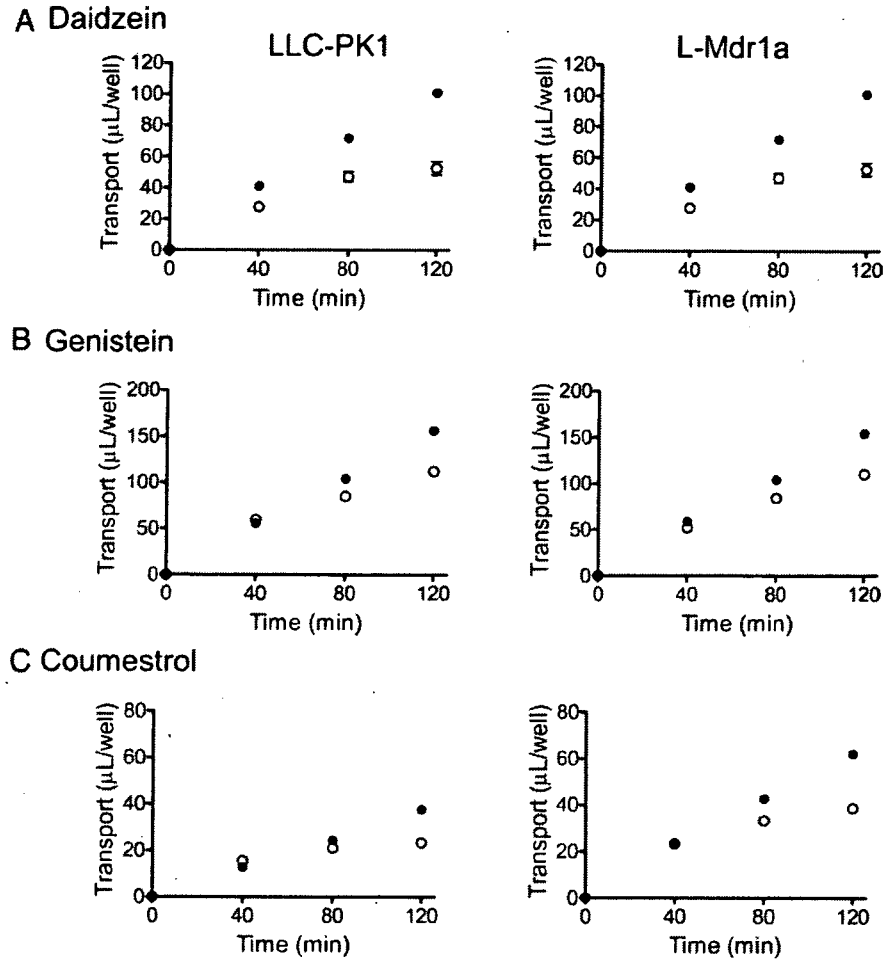

Fig. 2. The transcellular transport of daidzein (A), genistein (B), and coumestrol (C) across monolayers of control and mMdr1a-expressing LLC-PK1 cells. Transport in the apical-to-basal direction is represented by ○ and that in the basal-to-apical direction by ●. Data are represented by means ± S.E. of triplicate experiments.

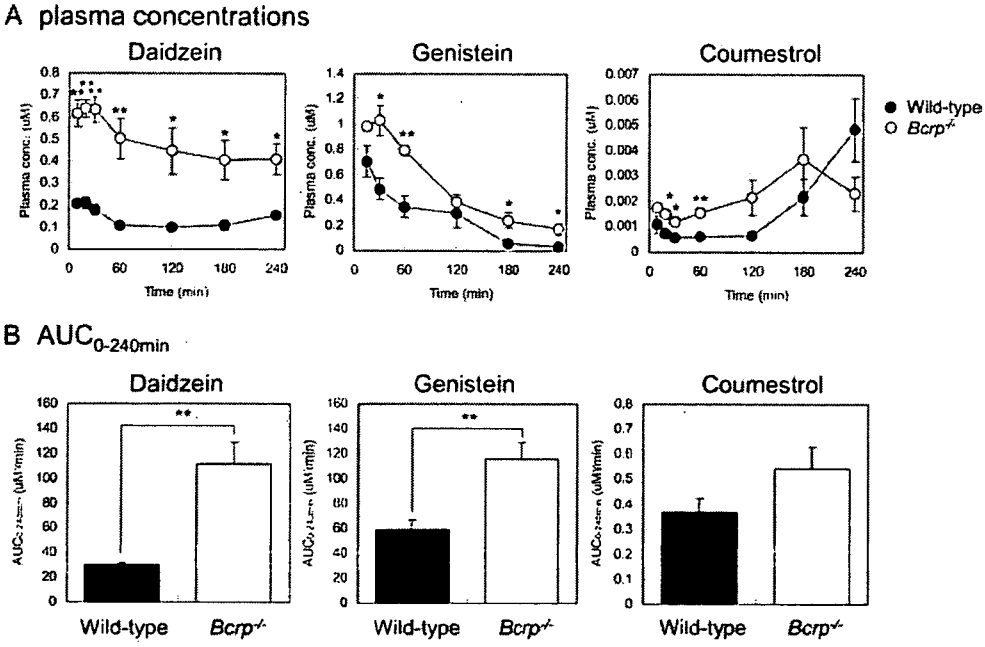

Fig. 3. Comparison of the plasma concentrations of daidzein, genistein, and coumestrol after oral administration (30 μmol/kg) of daidzein, genistein, or coumestrol between wild-type and *Bcrp*$^{-/-}$ mice. A, the time profiles of plasma concentrations. B, plasma AUC from time 0 to 240 min. Data are represented by means ± S.E. of three or four mice. Asterisks represent statistically significant differences between wild-type and *Bcrp*$^{-/-}$ mice: *, $P < 0.05$; **, $P < 0.01$.

only in the endothelial cells (Fig. 6A) and specifically in the luminal membrane (Fig. 6C). In the epididymis, the localization of Bcrp differed between the head and body regions (Fig. 6D). In the head (Fig. 6D, left), Bcrp was detected in both the luminal and abluminal sides of ducts, whereas in the body (Fig. 6D, right), Bcrp staining was observed in the endothelial cells. Immunofluorescence by BXP-53 was diminished in *Bcrp*$^{-/-}$ mice, indicating that the signals were associated specifically with Bcrp. We also examined the mRNA expression level of *BCRP* in the human epididymis. The ratio of *BCRP* mRNA to that of *GAPDH* was 1.16×10^{-2} and was similar to that found in the mouse epididymis (1.42×10^{-2}).

Role of Bcrp on the Accumulation of Genistein in the Fetus and Fetus Brain. Role of Bcrp on the fetal distribution of genistein was investigated in pregnant mice. Genistein was given to pregnant mice by constant intravenous infusion, and the plasma concentrations were similar between wild-type and *Bcrp*$^{-/-}$ mice (Fig. 7A). The fetus-to-maternal plasma concentration ratio was 1.8-fold greater in *Bcrp*$^{-/-}$ mice than controls (Fig. 7B). Brain-to-whole body concentration ratios were compared between wild-type and *Bcrp*$^{-/-}$ fetus to evaluate the Bcrp function in fetal blood-brain barrier. Brain-to-whole body concentration ratio was 1.4-fold increased in *Bcrp*$^{-/-}$ mice (Fig. 7C).

Discussion

In the present study, the role of Bcrp in limiting oral absorption of the phytoestrogens and their penetration into the brain, testis, epididymis, and fetus was investigated using *Bcrp*$^{-/-}$ mice. We tested three phytoestrogens, daidzein, genistein, and coumestrol. Daidzein and genistein are two major isoflavonoids in soy-based meal and are the most frequently ingested phytoestrogens. Coumestrol is known to be the most potent phytoestrogen. We found that all three phytoestrogens are substrates of Bcrp (Fig. 1). We also investigated the transport of the phytoestrogens by mMdr1a, which exhibits overlapped tissue distribution with Bcrp, and has been shown to limit the oral availability and tissue distributions of a variety of compounds. However, it was found that

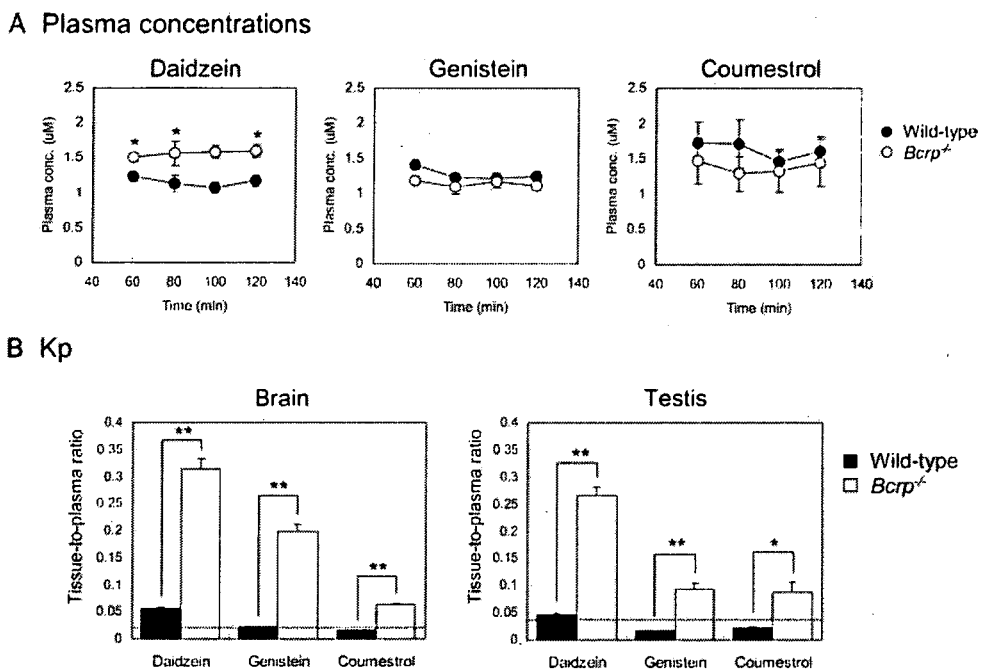

Fig. 4. Comparison of the brain and testis distributions of daidzein, genistein, or coumestrol between wild-type and *Bcrp*$^{-/-}$ mice. Compounds were infused intravenously at a dose rate of 5 μmol/h/kg, and K_p values in the brain and testis were measured at 120 min. A, the time profiles of plasma concentrations. B, K_p values in the brain and testis. K_p values of [^{14}C]inulin are represented by broken lines. Data are represented by means ± S.E. of three or four mice. Asterisks represent statistically significant differences between wild-type and *Bcrp*$^{-/-}$ mice; *, $P < 0.05$; **, $P < 0.01$.

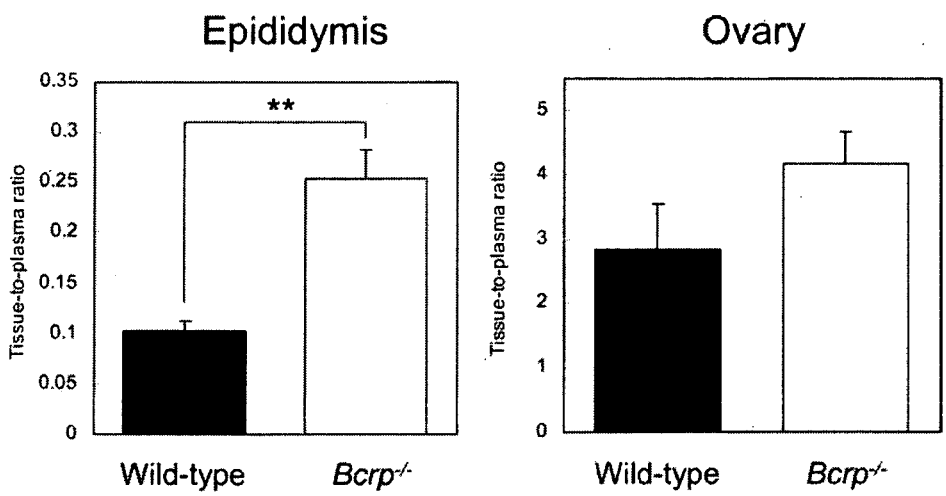

Fig. 5. Comparison of the epididymal and ovarian distributions of genistein between wild-type and *Bcrp*$^{-/-}$ mice. Genistein was infused intravenously at a dose rate of 5 μmol/h/kg, and K_p values in the epididymis and ovary were obtained at 120 min in male and female mice, respectively. Data are represented by means ± S.E. of three or four mice. Asterisks represent statistically significant differences between wild-type and *Bcrp*$^{-/-}$ mice: **, $P < 0.01$.

all three phytoestrogens were not the substrate of Mdr1a (Fig. 2).

After oral administration, the plasma AUC of daidzein and genistein was significantly increased in *Bcrp*$^{-/-}$ mice (Fig. 3, A and B). For coumestrol, the plasma concentrations exhibited a significant change in *Bcrp*$^{-/-}$ mice only at early time points, and thus, the AUC did not exhibit a statistically significant change. There are three potential sites to account for the increase in the plasma concentration after oral administration: an increase in intestinal absorption, and a decrease in intestinal and hepatic extraction. When given intravenously, the change in the plasma concentrations of phytoestrogens between wild-type and *Bcrp*$^{-/-}$ mice were marginal (Fig. 4). This is reasonable because the major elimination pathway of phytoestrogens from the systemic circulation is glucuronidation. Impaired Bcrp hardly affects the hepatic first-pass effect for phytoestrogens. Glucuronidation may be part of the mechanism limiting oral availability of the phytoestrogens as reported for quercetin (Crespy et al., 1999). We have reported that the intestinal glucuronidation activity of 4-methylumberifellone exhibited no change in *Bcrp*$^{-/-}$ mice (Enokizono et al., 2007). Therefore, the enhanced plasma exposure after oral administration in *Bcrp*$^{-/-}$ mice is probably due to an increased intestinal absorption. The effect of Bcrp on the oral availability of coumestrol was minimal, whereas the in vitro transport activity by mBcrp

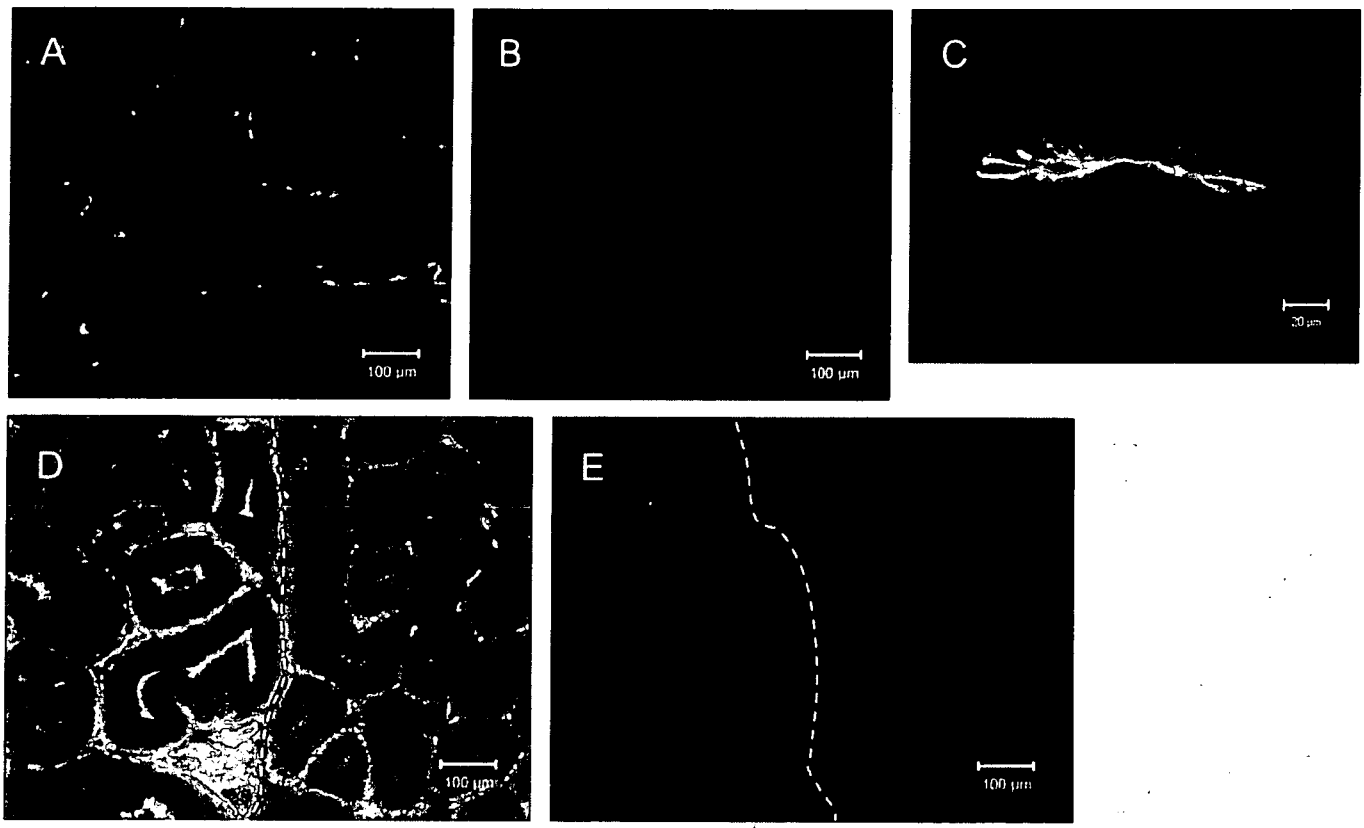

Fig. 6. Immunohistochemical analysis of Bcrp in the testis and epididymis. Localizations of Bcrp protein and DNA are shown by green and blue staining, respectively. A, testis of wild-type mice. B, testis of *Bcrp*$^{-/-}$ mouse. C, endothelial cells in the testis of wild-type mice. D, epididymis of wild-type mouse. E, epididymis of *Bcrp*$^{-/-}$ mouse. In D and E, the white lines discriminate the head (left) from the body (right).

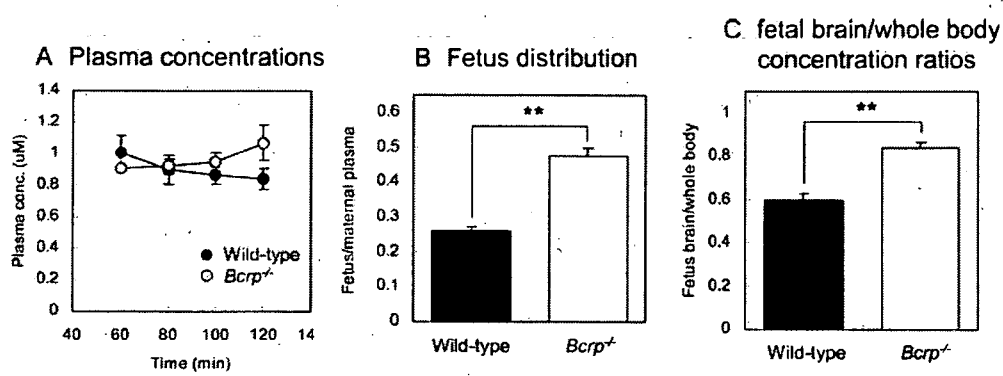

Fig. 7. Comparison of the distributions of genistein into the fetuses and fetal brain between wild-type and *Bcrp*$^{-/-}$ mice. Genistein was intravenously infused to pregnant mice at a dose rate of 5 μmol/h/kg, and the distributions into the fetuses and fetal brain were measured at 120 min. A, the time profiles of plasma concentrations. B, fetus-to-maternal plasma concentration ratios. C, brain-to-whole body concentration ratios in fetal mice. Data are represented by means ± S.E. of three mice. Asterisks represent statistically significant differences between wild-type and *Bcrp*$^{-/-}$ mice: **, $P < 0.01$.

was similar among the three phytoestrogens (Fig. 1). This indicates the smaller contribution of Bcrp to the intestinal absorption of coumestrol. The contribution of paracellular transport and intestinal metabolism may be greater for coumestrol than the other phytoestrogens. Indeed, transcellular transport of coumestrol in the apical-to-basal direction in control cells (MDCKII/GFP and LLC-PK1) was lowest among the three phytoestrogens, suggesting the lowest transcellular transport of coumestrol. The mechanism governing the increased plasma concentrations of daidzein during intravenous infusion in *Bcrp*$^{-/-}$ mice remains unknown. Impaired urinary excretion could be one possible mechanism because daidzein also undergoes urinary excretion: approximately 10% of the dose after oral administration (Bayer et al., 2001).

The K_p values of brain and testis of all three phytoestrogens were significantly increased in *Bcrp*$^{-/-}$ mice (Fig. 4B). Considering that the K_p values of the phytoestrogens and [^{14}C]inulin were similar in wild-type mice, the brain and testis distribution of the phytoestrogens is almost completely limited by Bcrp. Bcrp has been identified on the luminal membrane of both the human and mouse brain capillary endothelial cells that form the blood-brain barrier (Cooray et al., 2002; Lee et al., 2005), whereas there is an interspecies difference in membrane localization in the testis. Bcrp is localized on both the luminal side of the endothelial cells and the apical membrane of myoid cells in the human testis (Bart et al., 2004), whereas Bcrp expression is restricted to the luminal membrane of capillary-like structures in the mouse testis (Fig. 6, A and C). It is generally considered that the Sertoli and myoid cells form the blood-testis barrier, but endothelial cell-cell junctions are more leaky in rats (Dym and Fawcett, 1970). However, from the present results, testicular endothelial cells evidently have an adequate barrier function against phytoestrogens, at least in mice.

In addition to the testis, we investigated the role of Bcrp in other reproductive organs, the epididymis and ovary. The epididymis is divided into three segments (head, body, and tail). Sperm formed in the testis enter the head and finally reach the tail. During this transition, they undergo maturation and are finally stored in the tail region. It was found that the distribution of genistein was also increased in the epididymis of *Bcrp*$^{-/-}$ mice (Fig. 5). Therefore, we propose that Bcrp limits the penetration of genistein into the epididymis. The membrane localization of Bcrp was regionally dependent in the epididymis. Bcrp was mainly localized in capillary-like structures in the body (Fig. 6D, left), whereas Bcrp was found both in the luminal and abluminal membranes of the ducts in the head (Fig. 6D, right). Bcrp in the capillary-like structure and the abluminal membranes of ducts may contribute to the reduced distribution of genistein in wild-type mice. The physiological role of the Bcrp in the luminal membranes of the ducts in the head is unknown. It may mediate the luminal secretion of some endogenous compounds. Unlike male reproductive organs, the ovaries did not exhibit any change in the tissue distribution of genistein (Fig. 5), although the *Bcrp* mRNA level in the ovaries is similar to that in the testis (Tanaka et al., 2005). The reason for the discrepancy between mRNA expression and functional activity in the ovaries remains unknown.

Fetal and newborn mice are more sensitive to estrogen than adults. The distribution of genistein in the fetus was increased in pregnant *Bcrp*$^{-/-}$ mice (Fig. 7B), suggesting that Bcrp limits the penetration of genistein into the fetus in the placenta. Furthermore, the brain-to-whole body concentration ratio was also increased in fetal *Bcrp*$^{-/-}$ mice (Fig. 7C). Therefore, fetal brain capillaries may develop a barrier function to some degree even at this stage. The smaller increase (1.4-fold) than that observed in adult mice (9.2-fold) suggests that the barrier function is still immature at this stage (Nico et al., 1999). Taken together, the exposure of phytoestrogens to the fetal brain is limited by Bcrp in the fetal blood-brain barrier, the placenta, and the maternal small intestine.

Estrogen plays a key role in the development of reproductive systems, and sexual differentiation and estrogenic chemicals are known to influence reproductive functions, such as reduced testicular weight, sperm counts, induction of the acrosome reaction in both human and mouse (Atanassova et al., 2000; Adeoya-Osiguwa et al., 2003; Kyselova et al., 2004; Fraser et al., 2006), and adult sexual behavior, such as reduced mounting and ejaculation in males and reduced lordosis in females (Patisaul et al., 2004). Bcrp will prevent these adverse effects of phytoestrogens by limiting the exposure to the reproductive organs and brain.

In conclusion, we have demonstrated the importance of Bcrp in limiting the oral availability of phytoestrogens and their penetration into the brain and male reproductive organs. In addition, Bcrp also limited the exposure of the mouse fetus to phytoestrogens by extruding them to the blood from the placenta. These results indicate the important roles of Bcrp in protecting the body from the adverse effects of phytoestrogens on sexual behavior and spermatogenesis.

Acknowledgments

We thank Dr. Alfred H. Schinkel (The Netherlands Cancer Institute, The Netherlands) for supplying *Bcrp*$^{-/-}$ mice and L-Mdr1a cells.

References

Adeoya-Osiguwa SA, Markoulaki S, Pocock V, Milligan SR, and Fraser LR (2003) 17beta-Estradiol and environmental estrogens significantly affect mammalian sperm function. *Hum Reprod* **18**:100–107.

Adlercreutz H (1995) Phytoestrogens: epidemiology and a possible role in cancer protection. *Environ Health Perspect* **103 Suppl 7**:103–112.

Atanassova N, McKinnell C, Turner KJ, Walker M, Fisher JS, Morley M, Millar MR, Groome NP, and Sharpe RM (2000) Comparative effects of neonatal exposure of male rats to potent and weak (environmental) estrogens on spermatogenesis at puberty and the relationship to adult testis size and fertility: evidence for stimulatory effects of low estrogen levels. *Endocrinology* **141**:3898–3907.

Bart J, Hollema H, Groen HJ, de Vries EG, Hendrikse NH, Sleijfer DT, Wegman TD, Vaalburg W, and van der Graaf WT (2004) The distribution of drug-efflux pumps, P-gp, BCRP, MRP1 and MRP2, in the normal blood-testis barrier and in primary testicular tumours. *Eur J Cancer* **40**:2064–2070.

Bayer T, Colnot T, and Dekant W (2001) Disposition and biotransformation of the estrogenic isoflavone daidzein in rats. *Toxicol Sci* **62**:205–211.

Breedveld P, Pluim D, Cipriani G, Wielinga P, van Tellingen O, Schinkel AH, and Schellens JH (2005) The effect of Bcrp1 (Abcg2) on the in vivo pharmacokinetics and brain penetration of imatinib mesylate (Gleevec): implications for the use of breast cancer resistance protein and P-glycoprotein inhibitors to enable the brain penetration of imatinib in patients. *Cancer Res* **65**:2577–2582.

Breedveld P, Zelcer N, Pluim D, Sonmezer O, Tibben MM, Beijnen JH, Schinkel AH, van Tellingen O, Borst P, and Schellens JH (2004) Mechanism of the pharmacokinetic interaction between methotrexate and benzimidazoles: potential role for breast cancer resistance protein in clinical drug-drug interactions. *Cancer Res* **64**:5804–5811.

Cassidy A, Bingham S, and Setchell K (1995) Biological effects of isoflavones in young women: importance of the chemical composition of soybean products. *Br J Nutr* **74**:587–601.

Chang HC, Churchwell MI, Delclos KB, Newbold RR, and Doerge DR (2000) Mass spectrometric determination of Genistein tissue distribution in diet-exposed Sprague-Dawley rats. *J Nutr* **130**:1963–1970.

Chen J, Wang S, Jia X, Bajimaya S, Lin H, Tam VH, and Hu M (2005) Disposition of flavonoids via recycling: comparison of intestinal versus hepatic disposition. *Drug Metab Dispos* **33**:1777–1784.

Cooray HC, Blackmore CG, Maskell L, and Barrand MA (2002) Localisation of breast cancer resistance protein in microvessel endothelium of human brain: *Neuroreport* **13**:2059–2063.

Crespy V, Morand C, Manach C, Besson C, Demigne C, and Remesy C (1999) Part of quercetin absorbed in the small intestine is conjugated and further secreted in the intestinal lumen. *Am J Physiol* **277**:G120–G126.

Delclos KB, Bucci TJ, Lomax LG, Latendresse JR, Warbritton A, Weis CC, and Newbold RR (2001) Effects of dietary genistein exposure during development on male and female CD (Sprague-Dawley) rats. *Reprod Toxicol* **15**:647–663.

Doerge DR, Churchwell MI, Chang HC, Newbold RR, and Delclos KB (2001) Placental transfer of the soy isoflavone genistein following dietary and gavage administration to Sprague-Dawley rats. *Reprod Toxicol* **15**:105–110.

Dym M and Fawcett DW (1970) The blood-testis barrier in the rat and the physiological compartmentation of the seminiferous epithelium. *Biol Reprod* **3**:308–326.

Enokizono J, Kusuhara H, and Sugiyama Y (2007) Regional expression and activity of breast cancer resistance protein (ABCG2) in mouse intestine: overlapped distribution with sulfotransferases. *Drug Metab Dispos* **35**:922–928.

Fraser LR, Beyret E, Milligan SR, and Adeoya-Osiguwa SA (2006) Effects of estrogenic xenobiotics on human and mouse spermatozoa. *Hum Reprod* **21**:1184–1193.

Hirano M, Maeda K, Matsushima S, Nozaki Y, Kusuhara H, and Sugiyama Y (2005) Involvement of BCRP (ABCG2) in the biliary excretion of pitavastatin. *Mol Pharmacol* **68**:800–807.

Imai Y, Tsukahara S, Asada S, and Sugimoto Y (2004) Phytoestrogens/flavonoids reverse breast cancer resistance protein/ABCG2-mediated multidrug resistance. *Cancer Res* **64**:4346–4352.

Jonker JW, Buitelaar M, Wagenaar E, Van Der Valk MA, Scheffer GL, Scheper RJ, Plosch T, Kuipers F, Elferink RP, Rosing H, et al. (2002) The breast cancer resistance protein protects against a major chlorophyll-derived dietary phytotoxin and protoporphyria. *Proc Natl Acad Sci U S A* **99**:15649–15654.

Kondo C, Suzuki H, Itoda M, Ozawa S, Sawada J, Kobayashi D, Ieiri I, Mine K, Ohtsubo K, and Sugiyama Y (2004) Functional analysis of SNPs variants of BCRP/ABCG2. *Pharm Res* **21**:1895–1903.

Kyselova V, Peknicova J, Boubelik M, and Buckiova D (2004) Body and organ weight, sperm acrosomal status and reproduction after genistein and diethylstilbestrol treatment of CD1 mice in a multigenerational study. *Theriogenology* **61**:1307–1325.

Lee YJ, Kusuhara H, Jonker JW, Schinkel AH, and Sugiyama Y (2005) Investigation of efflux transport of dehydroepiandrosterone sulfate and mitoxantrone at the mouse blood-brain barrier: a minor role of breast cancer resistance protein. *J Pharmacol Exp Ther* **312**:44–52.

Maliepaard M, Scheffer GL, Faneyte IF, van Gastelen MA, Pijnenborg AC, Schinkel AH, van De Vijver MJ, Scheper RJ, and Schellens JH (2001) Subcellular localization and distribution of the breast cancer resistance protein transporter in normal human tissues. *Cancer Res* **61**:3458–3464.

Matsushima S, Maeda K, Kondo C, Hirano M, Sasaki M, Suzuki H, and Sugiyama Y (2005) Identification of the Hepatic efflux transporters of organic anions using double-transfected Madin-Darby canine kidney II cells expressing human organic anion-transporting polypeptide 1B1 (OATP1B1)/multidrug resistance-associated protein 2, OATP1B1/multidrug resistance 1, and OATP1B1/breast cancer resistance protein. *J Pharmacol Exp Ther* **314**:1059–1067.

Mizuno N, Suzuki M, Kusuhara H, Suzuki H, Takeuchi K, Niwa T, Jonker JW, and Sugiyama Y (2004) Impaired renal excretion of 6-hydroxy-5,7-dimethyl-2-methylamino-4-(3-pyridylmethyl) benzothiazole (E3040) sulfate in breast cancer resistance protein (BCRP1/ABCG2) knockout mice. *Drug Metab Dispos* **32**:898–901.

Mueller SO, Simon S, Chae K, Metzler M, and Korach KS (2004) Phytoestrogens and their human metabolites show distinct agonistic and antagonistic properties on estrogen receptor alpha (ERalpha) and ERbeta in human cells. *Toxicol Sci* **80**:14–25.

Nico B, Quondamatteo F, Herken R, Marzullo A, Corsi P, Bertossi M, Russo G, Ribatti D, and Roncali L (1999) Developmental expression of ZO-1 antigen in the mouse blood-brain barrier. *Brain Res Dev Brain Res* **114**:161–169.

Patisaul HB, Luskin JR, and Wilson ME (2004) A soy supplement and tamoxifen inhibit sexual behavior in female rats. *Horm Behav* **45**:270–277.

Setchell KD, Brown NM, Zimmer-Nechemias L, Brashear WT, Wolfe BE, Kirschner AS, and Heubi JE (2002) Evidence for lack of absorption of soy isoflavone glycosides in humans, supporting the crucial role of intestinal metabolism for bioavailability. *Am J Clin Nutr* **76**:447–453.

Sfakianos J, Coward L, Kirk M, and Barnes S (1997) Intestinal uptake and biliary excretion of the isoflavone genistein in rats. *J Nutr* **127**:1260–1268.

Smith AJ, Mayer U, Schinkel AH, and Borst P (1998) Availability of PSC833, a substrate and inhibitor of P-glycoproteins, in various concentrations of serum. *J Natl Cancer Inst* **90**:1161–1166.

Tanaka Y, Slitt AL, Leazer TM, Maher JM, and Klaassen CD (2005) Tissue distribution and hormonal regulation of the breast cancer resistance protein (Bcrp/Abcg2) in rats and mice. *Biochem Biophys Res Commun* **326**:181–187.

van Herwaarden AE, Jonker JW, Wagenaar E, Brinkhuis RF, Schellens JH, Beijnen JH, and Schinkel AH (2003) The breast cancer resistance protein (Bcrp1/Abcg2) restricts exposure to the dietary carcinogen 2-amino-1-methyl-6-phenylimidazo[4,5-b]pyridine. *Cancer Res* **63**:6447–6452.

Watanabe S, Terashima K, Sato Y, Arai S, and Eboshida A (2000) Effects of isoflavone supplement on healthy women. *Biofactors* **12**:233–241.

Whitten PL, Patisaul HB, and Young LJ (2002) Neurobehavioral actions of coumestrol and related isoflavonoids in rodents. *Neurotoxicol Teratol* **24**:47–54.

Wisniewski AB, Klein SL, Lakshmanan Y, and Gearhart JP (2003) Exposure to genistein during gestation and lactation demasculinizes the reproductive system in rats. *J Urol* **169**:1582–1586.

Zhang W, Mojsilovic-Petrovic J, Andrade MF, Zhang H, Ball M, and Stanimirovic DB (2003) The expression and functional characterization of ABCG2 in brain endothelial cells and vessels. *FASEB J* **17**:2085–2087.

Address correspondence to: Dr. Yuichi Sugiyama, Graduate School of Pharmaceutical Sciences, The University of Tokyo, 7-3-1, Hongo, Bunkyo-ku, Tokyo 113-0033, Japan. E-mail: sugiyama@mol.f.u-tokyo.ac.jp

0026-895X/07/7206-1619–1625
MOLECULAR PHARMACOLOGY
U.S. Government work not protected by U.S. copyright
Mol Pharmacol 72:1619–1625, 2007

Vol. 72, No. 6
39701/3277936
Printed in U.S.A.

Regulation of Tissue-Specific Expression of the Human and Mouse Urate Transporter 1 Gene by Hepatocyte Nuclear Factor 1 α/β and DNA Methylation

Ryota Kikuchi, Hiroyuki Kusuhara, Naka Hattori, Insook Kim, Kunio Shiota, Frank J. Gonzalez, and Yuichi Sugiyama

Department of Molecular Pharmacokinetics, Graduate School of Pharmaceutical Sciences, the University of Tokyo, Tokyo, Japan (R.K., H.K., Y.S.); Laboratory of Cellular Biochemistry, Department of Animal Resource Sciences/Veterinary Medical Sciences, the University of Tokyo, Tokyo, Japan (N.H., K.S.); Laboratory of Metabolism, National Cancer Institute, National Institutes of Health, Bethesda, Maryland (I.K., F.J.G.)

Received July 6, 2007; accepted September 10, 2007

ABSTRACT

Expression of Urate transporter 1 (URAT1/*SLC22A12*) is restricted to the proximal tubules in the kidney, where it is responsible for the tubular reabsorption of urate. To elucidate the mechanism underlying its tissue-specific expression, the transcriptional regulation of the *hURAT1* and *mUrat1* genes was investigated. Hepatocyte nuclear factor 1 α (HNF1α) and HNF1β positively regulate minimal promoter activity of the *URAT1* gene as shown by reporter gene assays. Electrophoretic mobility shift assays revealed binding of HNF1α and/or HNF1β to the HNF1 motif in the *hURAT1* promoter. Furthermore, the mRNA expression of Urat1 is reduced in the kidneys of *Hnf1*α-null mice compared with wild-type mice, confirming the indispensable role of HNF1α in the constitutive expression of *URAT1* genes. It was also shown that the proximal promoter region of *mUrat1* was hypermethylated in the liver and kidney medulla, whereas this region was relatively hypomethylated in the kidney cortex. These methylation profiles are in a good agreement with the proximal tubule-restricted expression of mUrat1 in the kidney cortex. Taken together, these results strongly suggest that tissue-specific expression of the *URAT1* genes is coordinately regulated by the transcriptional activation by HNF1α/HNF1β heterodimer and repression by DNA methylation.

Urate is an end product of purine metabolism in humans and other higher primates. It is generally recognized that urate works as a scavenger of potentially harmful radicals in the human body. However, hyperuricemia can be associated with health problems such as gout, nephrolithiasis, hypertension, and vascular disease, whereas hypouricemia is primarily characterized by exercise-induced acute renal failure. Thus, the serum urate level must be tightly regulated through complex renal handling processes, which is historically explained by a four-component model (i.e., glomerular filtration, tubular secretion, and pre- and postsecretory reabsorption). After these processes, approximately 90% of the urate filtered through the glomerulus is reabsorbed in humans (Rafey et al., 2003; Enomoto and Endou, 2005; Hediger et al., 2005).

Urate transporter 1 (URAT1/*SLC22A12*) is a membrane transporter responsible for the reabsorption of urate in the apical membrane of the renal proximal tubules (Enomoto et al., 2002). Mutations in the *URAT1* gene, causing functional impairment, are associated with idiopathic renal hypouricemia (Enomoto et al., 2002; Iwai et al., 2004). In addition, fractional excretion of urate in patients with homozygous or compound heterozygous *SLC22A12* mutations is not sensitive to uricosuric (probenecid and benzbromarone) and antiuricosuric (pyrazinamide) drugs, suggesting that these drugs target URAT1 to exert their effects in vivo (Ichida et al., 2004). The mouse homolog of hURAT1, mUrat1, shows the same tissue distribution as that of hURAT1 and is probably involved in the reabsorption of urate in the kidney (Hosoyamada et al., 2004). It can also be an exit pathway for

Article, publication date, and citation information can be found at http://molpharm.aspetjournals.org.
doi:10.1124/mol.107.039701.

ABBREVIATIONS: OAT, organic anion transporter; URAT1, urate transporter 1; HNF1, hepatocyte nuclear factor 1; PCR, polymerase chain reaction; Gapdh, glyceraldehyde-3-phosphate dehydrogenase; T-DMR, tissue-dependent differentially methylated region; MODY, maturity-onset diabetes of the young; HEK, human embryonic kidney; wt, wild-type hepatocyte nuclear factor 1 motif in the *hURAT1* promoter; per, the consensus sequence for the hepatocyte nuclear factor 1 motif; mut, mutated hepatocyte nuclear factor 1 motif; m, mouse; h, human.

several anionic drugs in the proximal tubules together with the basolateral uptake transporters [organic anion transporter (Oat) 1 and Oat3] (Imaoka et al., 2004).

A previous report suggested the presence of a hepatocyte nuclear factor 1 (HNF1) binding motif in the minimal promoter region of the *hURAT1* gene, which is conserved in the proximal promoters of rodent *Urat1* genes (Li et al., 2004). HNF1 is known to regulate transcription of many hepatic genes by forming homodimers or heterodimers between two isoforms, HNF1α and HNF1β (Mendel and Crabtree, 1991; Tronche and Yaniv, 1992). Their expression in the kidney and a renal Fanconi syndrome or polycystic kidney disease in *Hnf1*α- or kidney-specific *Hnf1*β-null mice, respectively, also imply a role for these transcription factors in the kidney (Pontoglio et al., 1996; Gresh et al., 2004). We have found recently that HNF1α/β is a potent transactivator of the human and mouse *OAT3* promoter (Kikuchi et al., 2006). Then it was reported that the mRNA levels of several drug transporters, including Oat1 and Oat3, are reduced in the kidney of *Hnf1*α-null mice, further confirming the involvement of HNF1α in the transcriptional regulation of drug transporters in the kidney (Maher et al., 2006). The functional importance of HNF1 in the regulation of the *URAT1* gene has yet to be investigated. However, considering that the serum levels of urate are reduced and the renal fractional excretion is increased in *Hnf1*α-null mice (Pontoglio et al., 1996), it is possible that HNF1α directly regulates URAT1 expression.

HNF1α and HNF1β are expressed in the polarized epithelia of a variety of tissues, including liver, kidney, intestine, stomach, and pancreas (Blumenfeld et al., 1991; De Simone et al., 1991). Thus, positive regulation by HNF1 alone cannot account for the predominant expression of URAT1 in the kidney. Our previous study suggests that the expression of hOAT3 is negatively regulated by DNA methylation in addition to the positive regulation by HNF1α and HNF1β (Kikuchi et al., 2006). DNA methylation is one of the most well-characterized mechanisms underlying the epigenetic regulation of gene expression (Bird, 2002; Shiota, 2004). Methylation of the cytosine residue in the CpG dinucleotide negatively regulates gene transcription through the recruitment of chromatin remodeling factors, and many reports highlight the key role of DNA methylation in tissue-specific gene transcription. Because several CpG dinucleotides were found in the 5′-flanking region of *hURAT1* and *mUrat1* (Fig. 1), it is of great interest to determine whether the concerted effect of DNA methylation and HNF1α/β regulates tissue-specific expression of these genes. The present study was aimed to clarify the involvement of HNF1α and HNF1β as genetic factors and DNA methylation as an epigenetic factor in the tissue-specific expression of human and mouse *URAT1* genes.

Materials and Methods

Isolation of the 5′-Flanking Sequence of *hURAT1* and *mUrat1* Gene. The minimal promoter region of *hURAT1* gene (−253/+83) (Li et al., 2004) was amplified by PCR using human genomic DNA as a template and the forward (h − 253) and reverse (h + 83) primers with an artificial KpnI and HindIII site, respectively (Table 1). The PCR product was subcloned into the KpnI and HindIII restriction sites of pGL3-Basic (Promega, Madison, WI), yielding the *hURAT1* minimal promoter construct, hURAT1_−253/+83-HNF1wt. The transcriptional start site of the *mUrat1* gene was determined using the public database Database of Transcriptional Start Sites (available at http://dbtss.hgc.jp/) with the ref sequence identification for mUrat1 (NM_009203), and based on high homology with the 5′-flanking region of *hURAT1* (Fig. 1). Because the position of transcriptional start site in the clone MS2926204 is nearest to that of *hURAT1* transcriptional start site, which was experimentally determined in the previous report, we chose this site as the transcriptional start site of *mUrat1* gene. The *mUrat1* putative promoter region was isolated from mouse genomic

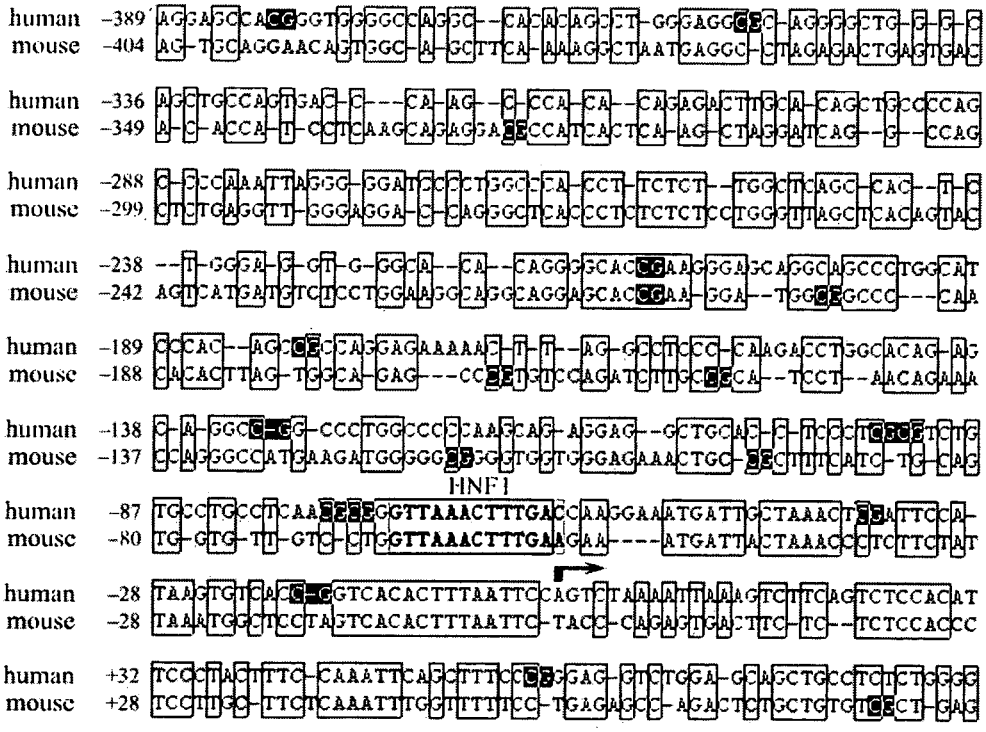

Fig. 1. Alignment of the proximal promoter of human and mouse *URAT1*. Nucleotide sequences of the proximal promoter region of human and mouse *URAT1* genes were aligned using Genetyx version 8 to show the high homology of the 5′-flanking region between species. Nucleotide numberings are relative to the transcriptional start sites indicated by an arrow (+1), and homologous sequences between species are boxed. Canonical HNF1 binding motif in the promoter is shaded, and CpG dinucleotides in each sequence are reverse-colored.

DNA by a PCR-based approach using the forward (m − 261) and reverse (m + 80) primers (Table 1). The PCR product was subcloned into pGL3-Basic as described above, yielding mUrat1_−260/+80. The sequences of all constructs were verified by DNA sequencing.

Site-Directed Mutagenesis. Mutations in the HNF1 motif located within the *hURAT1* minimal promoter were introduced using the QuikChange XL Site-Directed Mutagenesis Kit (Stratagene, La Jolla, CA) with internal mutated oligonucleotides (Table 1). The introduction of mutations was verified by DNA sequencing.

RNA Isolation and Quantitative PCR. Total RNA was isolated from the kidneys of 7- to 14-week-old male (n = 3) and female (n = 4) wild-type or *Hnf1α*-null adult mice (Lee et al., 1998) and treated with DNase I to remove the contaminated genomic DNA, followed by reverse-transcription using a random-nonamer primer (Takara, Shiga, Japan). To quantify the mRNA expression of mUrat1 in wild-type or *Hnf1α*-null mice, real-time quantitative PCR was performed as described previously using the primers shown in Table 1 (Kikuchi et al., 2006). The mRNA expression of mUrat1 was normalized by the mRNA expression of Gapdh and statistically analyzed by Student's t test. Asterisks (* and **) represent significant differences ($P < 0.05$ and $P < 0.01$, respectively) between wild-type and *Hnf1α*-null mice of each gender.

Cell Culture and Transfections. Cell culture, transfections, and luciferase assays were performed as described previously (Kikuchi et al., 2006). For transactivation assays in HEK293 cells, 5 ng of empty pcDNA3.1(+) vector, 5 ng of HNF1α expression vector, 2.5 ng of HNF1α and HNF1β expression vectors, or 5 ng of HNF1β expression vector was cotransfected with 0.5 μg of the corresponding promoter construct and 0.05 μg of internal standard pRL-SV40. The promoter activity was measured as relative light units of firefly luciferase per unit of *Renilla reniformis* luciferase.

Preparation of Nuclear Extracts and Electrophoretic Mobility Shift Assay. Nuclear extracts were prepared from HepG2, Caco-2, and HEK293 parent cells, or HEK293 cells transiently transfected with pcDNA3.1(+), either HNF1α or HNF1β expression vector, or both expression vectors as described previously (Kikuchi et al., 2006). Transient transfection of the expression vectors into HEK293 cells was performed using FuGENE6 (Roche Diagnostics, Indianapolis, IN) according to the manufacturer's instructions. Three kinds of double-stranded oligonucleotides (wt, per, and mut) were obtained by hybridizing the single-stranded complementary oligonucleotide with sense sequences shown in Table 1. Sequence "wt" corresponds to the wild-type HNF1 motif in the *hURAT1* promoter, and "per" corresponds to the perfect consensus sequence for the HNF1 motif, whereas "mut" denotes the wild-type sequence mutated within the motif. Five micrograms of nuclear extracts from HepG2, Caco-2, or HEK293 parent cells or 3 μg of nuclear extracts form HEK293 cells transfected with several expression vectors was used in the electrophoretic mobility shift assays. Competition and supershift assays were performed as described previously with Dig Gel Shift Kit, Second Generation (Roche Diagnostics).

Sodium Bisulfite Genomic Sequencing. Genomic DNA from liver, kidney cortex, or kidney medulla of ddY male mice at 8 weeks of age was extracted using a Get Pure DNA Kit (Dojindo Molecular Technologies, Gaithersburg, MD). One microgram of genomic DNA digested with EcoRI was denatured by adding NaOH to give a final concentration of 0.3 M and was incubated for 15 min at 37°C. After the incubation, sodium metabisulfite, pH 5.0, and hydroquinone were added to give final concentrations of 2.0 M and 0.5 mM, respectively, and the mixture was incubated for 16 h at 55°C in the dark. The modified DNA was purified using the Wizard DNA Clean-Up System (Promega), and the bisulfite reaction was terminated by adding NaOH to give a final concentration of 0.3 M and incubating for 15 min at 37°C. The solution was neutralized by adding NH_4OAc, pH 7.0, and the DNA was ethanol-precipitated, dried, and resuspended in 10 mM Tris-HCl and 1 mM EDTA, pH 8.0. The DNA fragment covering the proximal promoter region of the *mUrat1* gene was amplified by PCR using the following primers: −419-B-F, and +134-B-R (Table 1). The PCR products were cloned into pGEM-T Easy vector (Promega), and 10 clones randomly picked from each of two independent PCRs were sequenced to determine the presence of methylated cytosines.

TABLE 1

Oligonucleotides used for the production of promoter fragments, mobility shift assays, site-directed mutagenesis, quantitative PCR, and bisulfite PCR

Regarding the oligonucleotides used for the mobility shift assays and site-directed mutagenesis, the HNF1-motif in the *hURAT1* promoter region is underlined. Boldface type indicates the difference in the sequence of the per and mut compared with the wild-type sequence found in the *hURAT1* promoter.

Oligonucleotide	Orientation	Sequence (5′ to 3′)
Primers used for the cloning of 5′-flanking regions		
hURAT1		
h − 253	Forward	CGGGGTACCTTGGCTCAGCCACTCTGGGAGGT
h + 83	Reverse	CCCAAGCTTAGAGAGGCAGCTGCTCCAGACC
mUrat1		
m − 261	Forward	CGGGGTACCCTGGGTTAGCTCACAGTACAG
m + 80	Reverse	CCCAAGCTTAGCGACACAGCAGAGTCTG
Oligonucleotides used for the construction of EMSA probe and competitor or site-directed mutagenesis		
wt	Sense	CTCAACGCGGGTTAAACTTTGACCAAGGAAATG
per	Sense	CTCAACGCGGGTTAA**T**CA**T**TAACCAAGGAAATG
mut	Sense	CTCAACGCGGG**GGCG**AACT**G**TGACCAAGGAAATG
Primers used for quantitative PCR		
mUrat1	Forward	GAGGGAGACACGTTGACCAT
	Reverse	AAGTCCACAATCCCGATGAG
mGapdh	Forward	AACGACCCCTTCATTGAC
	Reverse	TCCACGACATACTCAGCAC
Primers used for bisulfite PCR		
mUrat1		
−419-B-F	Forward	GGGAATTAATAAGGGAGTGTAGGAA
+134-B-R	Reverse	TCACCATAAAACCTAAAACCCTCT

EMSA, electrophoretic mobility shift assay.

Results

Involvement of HNF1α/β in the Promoter Activity of *URAT1* Genes. A previous report suggested the presence of *cis*-elements required for the basal promoter activity of the *hURAT1* gene in the region from −253 to −39 base pairs relative to the transcriptional start site (Li et al., 2004). The minimal promoter construct of *hURAT1* was transfected into three human-derived cell lines, and luciferase activities were measured. The *hURAT1* promoter showed a significant increase in luciferase activity compared with the promoterless pGL3-Basic plasmid in HepG2 and Caco-2 cells, whereas the promoter activity was negligible in HEK293 cells (Fig. 2A).

To investigate the involvement of HNF1α or HNF1β in the *hURAT1* minimal promoter, the HNF1 motif found in the *hURAT1* promoter was disrupted by site-directed mutagenesis, and the promoter activity was measured in HepG2 and Caco-2 cells in which endogenous HNF1α and/or HNF1β is expressed (Kikuchi et al., 2006). Mutation in the HNF1 motif completely abolished the promoter activity in both cell lines (Fig. 2B). Direct confirmation of the importance of HNF1α or HNF1β for the promoter activity of *URAT1* genes was obtained by cotransfection assays in HEK293 cells in which neither HNF1α nor HNF1β is endogenously expressed (Fig. 2C). Exogenous expression of HNF1α and/or HNF1β markedly increased luciferase activity of the *hURAT1* wild-type reporter (−253/+83-HNF1wt) compared with the pcDNA3.1(+)-transfected control, whereas the luciferase activity of pGL3-Basic was unaffected. The luciferase activity driven by *hURAT1* HNF1-

mutated reporter (−253/+83-HNF1mut) was not transactivated by exogenously expressed HNF1α and/or HNF1β to the same degree as that of the wild-type construct as expected. The activity of *mUrat1* promoter (mUrat1_−261/+80) was also stimulated by forced expression of HNF1α and/or HNF1β. These results strongly suggest that the minimal promoter activity of human and mouse *URAT1* genes predominantly depends on the function of HNF1α or HNF1β.

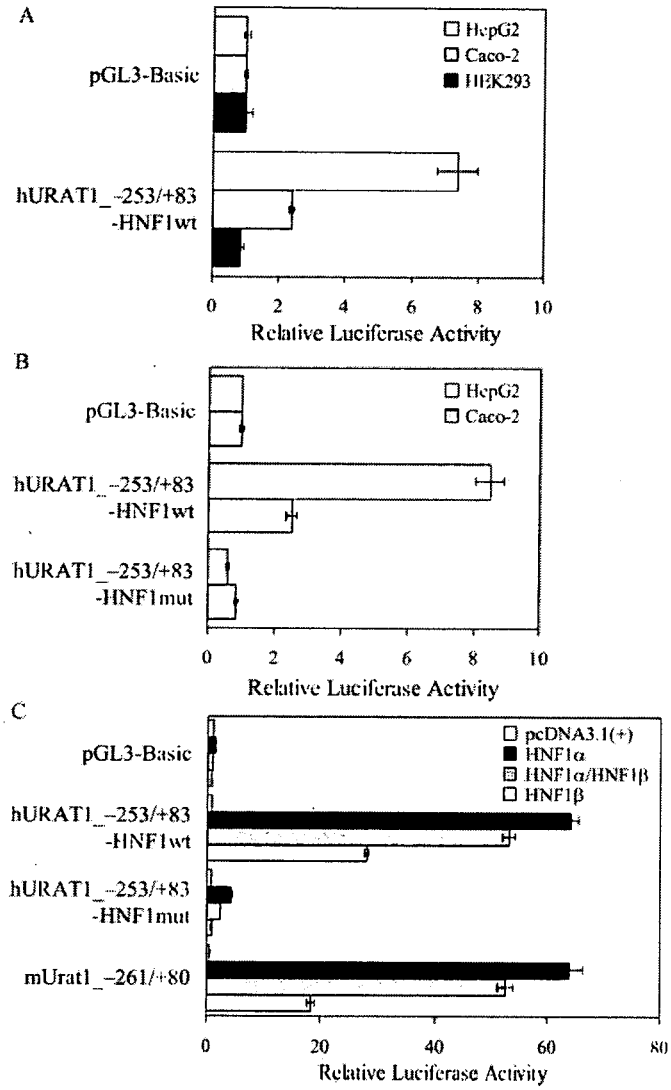

Fig. 2. HNF1α and HNF1β predominantly regulate *URAT1* promoters. A, analysis of *hURAT1* minimal promoter. HepG2 (□), Caco-2 (▨), and HEK293 cells (■) were transiently transfected with promoterless pGL3-Basic plasmid or minimal promoter construct of *hURAT1* (hURAT1_−253/+83-HNF1wt) together with the internal standard pRL-SV40 to normalize the transfection efficiency. B, mutational analysis of the HNF1 motif. HepG2 (□) and Caco-2 cells (▨) were transfected with pGL3-Basic, wild-type (hURAT1_−253/+83-HNF1wt), or HNF1-mutated (hURAT1_−253/+83-HNF1mut) promoter construct. C, exogenous expression of HNF1α and HNF1β. HEK293 cells were transfected with pGL3-Basic, wild-type, or the HNF1-mutated promoter construct of *hURAT1* (hURAT1_−253/+83-HNF1wt or hURAT1_−253/+83-HNF1mut, respectively), or the *mUrat1* promoter construct (mUrat1_−261/+80), together with empty pcDNA3.1(+) vector (white bars), HNF1α expression vector (black bars), HNF1α and HNF1β expression vectors (gray bars), or HNF1β expression vector (light gray bars). The promoter activity was measured as described under *Materials and Methods* and was shown as the induction factor over the background activity measured in cells transfected with pGL3-Basic in each cell line (A and B) or cells transfected with pGL3-Basic together with pcDNA3.1(+) (C). All results are presented as the mean ± S.E. of triplicate samples.

Interaction of HNF1α/β with the *hURAT1* Promoter. Interaction of digoxigenin-labeled oligonucleotide probes (wt, per, and mut) with nuclear proteins of HepG2, Caco-2, or HEK293 cells was assessed by electrophoretic mobility shift assays. The wt probe corresponds to the wild-type HNF1 motif in the *hURAT1* promoter, and the per probe corresponds to the consensus sequence for the HNF1 motif, whereas the mut probe has the same mutation in the HNF1 motif as that used in the luciferase assays. A nonspecific band, which was formed with every probe and abolished by 25-fold molar excess of both per and mut competitor, was observed in all cell lines. In the competition assays (Fig. 3A), one (band *a*) or two shifted bands (bands *a* and *b*) were formed with nuclear extracts derived from HepG2 or Caco-2 cells, respectively, when the wt and per probe were used (lanes 1, 4, 6, and 9). The bands *a* and *b* were abolished by an excess of unlabeled per but not by mut oligonucleotide (lanes 2, 3, 7, and 8), and these bands were not formed when the mut probe was used (lanes 5 and 10). These results suggest that bands *a* and *b* represent the binding of HNF1α or HNF1β to the HNF1 motif in the *hURAT1* promoter. In contrast, there were no specific bands in HEK293 cells (lanes 11 and 12), consistent with the lack of HNF1α and HNF1β in this cell line.

Supershift analysis with antibodies against HNF1α or HNF1β revealed specific interaction of HNF1α and/or HNF1β with the HNF1 motif in the *hURAT1* promoter (Fig. 3B). Addition of an anti-HNF1α antibody supershifted band *a* in HepG2 cells (lanes 3 and 4) and bands *a* and *b* in Caco-2 cells (lanes 8 and 9). Addition of an anti-HNF1β antibody resulted in the supershift of band *b* in Caco-2 cells (lanes 10 and 11), whereas band *a* was not supershifted (lanes 5, 6, 10, and 11). These results suggest that the bands *a* and *b* reflect the binding of HNF1α/HNF1α homodimer and HNF1α/HNF1β heterodimer, respectively. Binding of exogenously expressed HNF1α or HNF1β to the HNF1 motif was also demonstrated. Another shifted band showing faster mobility than HNF1α/HNF1β heterodimer was detected when the nuclear extracts of HEK293 cells transfected with HNF1β alone were incubated with the labeled probe, and this band was supershifted by anti-HNF1β antibody but not by anti-HNF1α antibody (data not shown). This result suggests that HNF1β/HNF1β homodimer can also interact with the HNF1 motif in the *hURAT1* promoter.

Impaired Expression of mUrat1 in *Hnf1α*-Null Mice. Real-time PCR analysis revealed that the expression of mUrat1 mRNA in the kidney is much lower in *Hnf1α*-null mice compared with wild-type mice of both genders (Fig. 4). In contrast to a previous report (Hosoyamada et al., 2004), there was no significant difference in the expression level of mUrat1 between male and female wild-type mice. On the other hand, the expression of mUrat1 mRNA in male mice was significantly higher than that in female in *Hnf1α*-null mice. The difference in *Hnf1α*-dependent expression (wild-type minus *Hnf1α*-null mice) between male and female mice did not reach statistical significance.

Epigenetic Regulation of the *mUrat1* Gene. Eight CpG dinucleotides, primary targets of DNA methylation in the vertebrate genome, are located in the 5′-flanking sequence up to −500 base pairs of *mUrat1* gene; seven of them

are within the minimal promoter region (Fig. 1). To elucidate the role of DNA methylation in the tissue-specific expression of the *mUrat1* gene, the methylation status of each CpG site was analyzed by sodium bisulfite genomic sequencing in the liver, kidney cortex, and kidney medulla, and the total methylation profiles in these tissues were compared (Fig. 5). These CpGs were heavily methylated in the liver and kidney medulla, in which there is no expression of mUrat1. In contrast, the region was relatively hypomethylated in the kidney cortex, in which mUrat1 is predominantly expressed. These results suggest that tissue-specific expression of *mUrat1* gene is regulated through DNA methylation-mediated gene silencing, and the proximal promoter region of the *mUrat1* gene can be regarded as a tissue-dependent differentially methylated region (T-DMR).

Discussion

In the present study, the involvement of both genetic and epigenetic mechanisms in the transcriptional regulation of human and mouse *URAT1* genes was demonstrated. A pivotal role for HNF1α and HNF1β in the minimal promoter activity of *URAT1* genes was confirmed by reporter gene assays (Fig. 2), and interaction of HNF1α/HNF1α homodimer, HNF1α/HNF1β heterodimer, and HNF1β/HNF1β homodimer with the HNF1 motif in the *hURAT1* promoter was shown by electrophoretic mobility shift assays (Fig. 3).

In the kidney, HNF1α normally exists as a heterodimer with HNF1β, although the HNF1α/HNF1α homodimer is a more potent transactivator than the heterodimer in vitro. HNF1β/HNF1β homodimer is also detectable in nuclear extracts from kidney, but the transactivation potency is the lowest among the three species (Rey-Campos et al., 1991; Pontoglio et al., 1996). Because expression of HNF1α is confined to the proximal tubules whereas that of HNF1β is observed along the entire nephron (Lazzaro et al., 1992; Pontoglio et al., 1996), formation of HNF1α/HNF1β heterodimer will be restricted to the proximal tubules in the kidney, and that of HNF1β/HNF1β homodimer is possible in the entire nephron. The expression of human and mouse *URAT1* genes is predominantly in the proximal tubules (Enomoto et al., 2002; Hosoyamada et al., 2004), which is consistent with the distribution of the HNF1α/HNF1β heterodimer. This suggests that the HNF1α/HNF1β heterodimer is required for constitutive expression of human and mouse URAT1. In contrast, the contribution of HNF1β/HNF1β homodimer is debatable. Although the HNF1β/HNF1β homodimer can also transactivate the *mUrat1* promoter, the expression of mUrat1 was markedly reduced in the kidney of *Hnf1α*-null mice (Fig. 4). This supports an essential role for the HNF1α/HNF1β heterodimer, which could not be compensated for by the HNF1β/HNF1β homodimer.

Eight CpG dinucleotides in the 5′-flanking region of the *mUrat1* gene appeared hypermethylated in the liver and kidney medulla, whereas they were relatively hypomethylated in the kidney cortex (Fig. 5). Two mechanisms are proposed for DNA methylation-dependent gene silencing: 1) DNA methylation directly interrupts the binding of transcription factors to their recognition sequences, including the CpG dinucleotide; and 2) methyl CpG binding proteins bound to the methylated cytosine recruit chromatin remodeling factors, such as histone deacetylases, and cause the neighboring chromatin configuration to condense, thereby preventing many transcription factors from accessing their recognition sequences within that region (Shiota, 2004). The HNF1 motif in the *mUrat1* promoter is located within the T-DMR, but the motif itself does not contain the CpG dinucleotide. It is possible that methylation of DNA in the T-DMR indirectly inhibits the binding of HNF1α or HNF1β to the promoter through chromatin remodeling events. Hypermethylation of the T-DMR may explain the absence of mUrat1 expression regardless of the formation of HNF1α/HNF1α homodimers in the liver. In the kidney, the promoter region is hypomethylated in the cortex but hypermethylated in the medulla. Together with the proximal tubule-restricted distribution of the HNF1α/HNF1β heterodimer, the regional difference in the methylation status seems to lead to the constitutive expression of mUrat1 in the proximal tubules in the cortex. In humans, the methylation profiles of *hURAT1* promoter re-

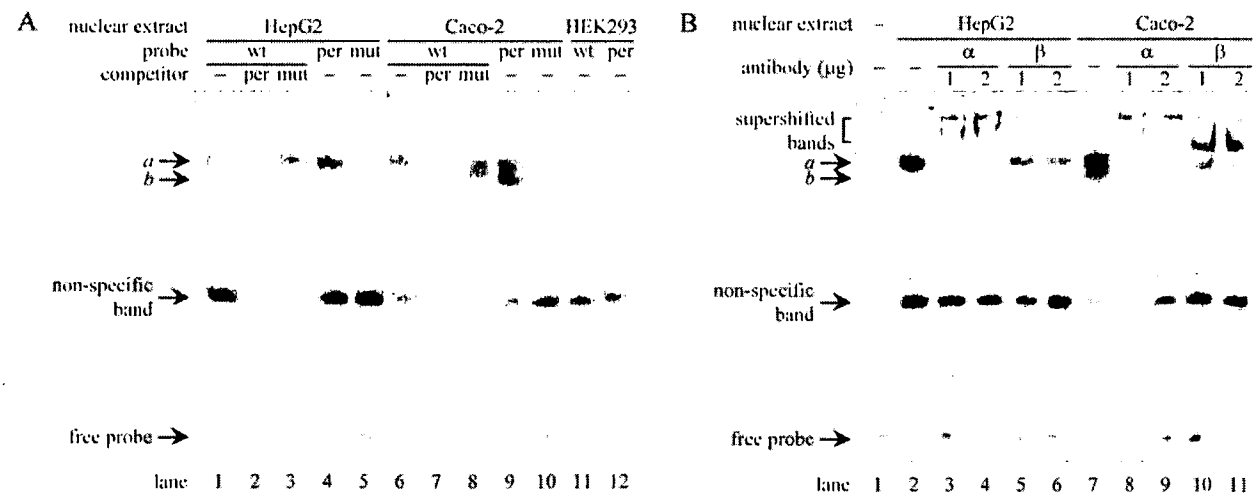

Fig. 3. HNF1α and HNF1β interact with the *hURAT1* promoter. A, competition assays. Three kinds of digoxigenin-labeled probe (Table 1) were incubated with nuclear extracts of HepG2, Caco-2, or HEK293 cells, with or without a 25-fold excess of unlabeled competitor (per or mut) as indicated. B, supershift assays. The wt probe was incubated with nuclear extracts of HepG2 or Caco-2 cells with or without an increasing amount of specific antibody against HNF1α (α) or HNF1β (β) as indicated. The DNA-protein complex was detected as described under *Materials and Methods*.

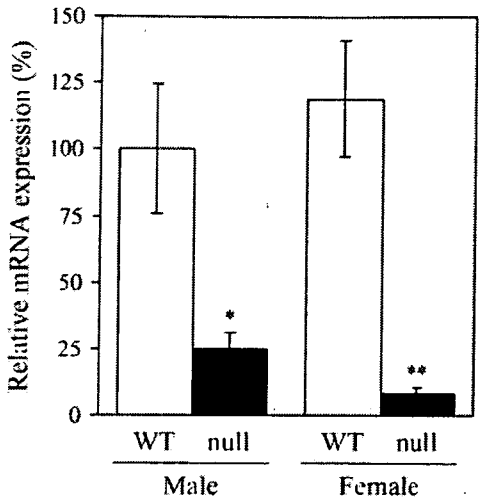

Fig. 4. Relative mRNA expression of mUrat1 in wild-type and *Hnf1α*-null mice. mRNA expression of mUrat1 in the kidneys of male or female wild-type (WT, □) and *Hnf1α*-null mice (null, ■) was measured by real-time quantitative PCR using specific primers (Table 1), and the data were normalized by the mRNA expression of Gapdh. The relative mRNA expression was given as a ratio with respect to the mRNA expression of mUrat1 in male wild-type mice that was taken as 100%. Results are presented as the mean ± S.E. of three (male) or four (female) mice. *, $P < 0.05$, and **, $P < 0.01$, significantly different between wild-type and *Hnf1α*-null mice.

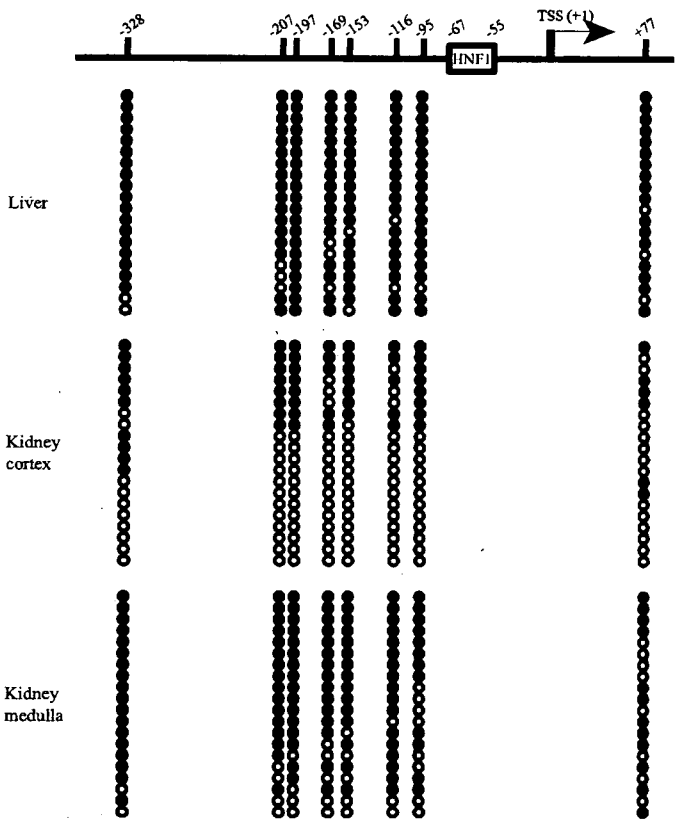

Fig. 5. DNA methylation profile of the *mUrat1* promoter. Top, a schematic diagram of the *mUrat1* 5′-flanking region. The vertical lines and numbers indicate the positions of cytosine residues of CpGs relative to the transcriptional start site (TSS, +1). The position of the HNF1 motif is shown by a rectangle. Bottom, DNA methylation status of individual CpGs. Bisulfite sequencing analysis was performed with genomic DNAs extracted from mouse liver, kidney cortex, and kidney medulla. ○ and ● represent unmethylated and methylated cytosines, respectively.

main unknown. Considering the similar frequency of CpG dinucleotides in the minimal promoter region between human and mouse (Fig. 1), DNA methylation will be also involved in the tissue/region-specific expression of hURAT1.

Mice lacking HNF1α suffer from severe renal Fanconi syndrome, a dysfunction in renal proximal tubular reabsorption (Pontoglio et al., 1996). The renal fractional excretion of urate is higher in mutant animals compared with wild-type controls, resulting in a lower serum urate level. In the present study, in vitro and in vivo evidence of the importance of HNF1α in the expression of *URAT1* genes was provided; accurate tissue-specific expression of this gene is essential for the reabsorption of filtered urate in the kidney. The altered renal excretion of urate in mutant mice is thus accounted for by impaired expression of Urat1. It was reported that expression of transporters responsible for reabsorption of filtered glucose, phosphate, and bile acids is also absent or lower in *Hnf1α*-null mice (Pontoglio et al., 2000; Shih et al., 2001; Cheret et al., 2002). Taken together, the expression of transporters required for the reabsorption of filtered solutes in the kidney proximal tubules is largely impaired in mutant mice, leading to renal Fanconi syndrome.

In addition to renal Fanconi syndrome, *Hnf1α*-null mice exhibit a phenotype similar to non–insulin-dependent diabetes mellitus (Lee et al., 1998; Pontoglio et al., 1998). In humans, mutations in HNF1α and HNF1β cause maturity-onset diabetes of the young (MODY) types 3 and 5, respectively (Yamagata et al., 1996; Horikawa et al., 1997). MODY is an autosomal dominant inherited disease that is responsible for 2 to 5% of non–insulin-dependent diabetes mellitus (Ledermann, 1995), and MODY3 accounts for 20 to 75% of patients with MODY, whereas MODY5 is a rare condition (Froguel and Velho, 1999; Winter and Silverstein, 2000; Ryffel, 2001). It was reported that the serum urate levels are low in patients with both type I and type II diabetes mellitus because of the elevated renal clearance (Shichiri et al., 1987; Magoula et al., 1991; Golik et al., 1993). The increase in the urate clearance has been ascribed to an elevated glomerular filtration rate and/or a defect in tubular urate reabsorption. It is thus possible that the expression of URAT1 mRNA is reduced in patients with MODY3 and MODY5, resulting in hypouricemia.

In conclusion, clear evidence is provided for the involvement of both genetic (HNF1α and HNF1β) and epigenetic (DNA methylation) mechanisms in establishing the tissue-specific expression of mouse and probably human *URAT1* genes. This is the first demonstration of the presence of T-DMR in the promoter region as far as transporters in the kidney are concerned.

Acknowledgments

We thank Dr. Shun Sato for his technical assistance and helpful discussions.

References

Bird A (2002) DNA methylation patterns and epigenetic memory. *Genes Dev* **16**:6–21.

Blumenfeld M, Maury M, Chouard T, Yaniv M, and Condamine H (1991) Hepatic nuclear factor 1 (HNF1) shows a wider distribution than products of its known target genes in developing mouse. *Development* **113**:589–599.

Cheret C, Doyen A, Yaniv M, and Pontoglio M (2002) Hepatocyte nuclear factor 1 alpha controls renal expression of the Npt1-Npt4 anionic transporter locus. *J Mol Biol* **322**:929–941.

De Simone V, De Magistris L, Lazzaro D, Gerstner J, Monaci P, Nicosia A, and

Cortese R (1991) LFB3, a heterodimer-forming homeoprotein of the LFB1 family, is expressed in specialized epithelia. *EMBO J* **10**:1435–1443.
Enomoto A and Endou H (2005) Roles of organic anion transporters (OATs) and a urate transporter (URAT1) in the pathophysiology of human disease. *Clin Exp Nephrol* **9**:195–205.
Enomoto A, Kimura H, Chairoungdua A, Shigeta Y, Jutabha P, Cha SH, Hosoyamada M, Takeda M, Sekine T, Igarashi T, et al. (2002) Molecular identification of a renal urate anion exchanger that regulates blood urate levels. *Nature* **417**: 447–452.
Froguel P and Velho G (1999) Molecular genetics of maturity-onset diabetes of the young. *Trends Endocrinol Metab* **10**:142–146.
Golik A, Weissgarten J, Cotariu D, Cohen N, Zaidenstein R, Ramot Y, Averbukh Z, and Modai D (1993) Renal uric acid handling in non-insulin-dependent diabetic patients with elevated glomerular filtration rates. *Clin Sci (Lond)* **85**:713–716.
Gresh L, Fischer E, Reimann A, Tanguy M, Garbay S, Shao X, Hiesberger T, Fiette L, Igarashi P, Yaniv M, et al. (2004) A transcriptional network in polycystic kidney disease. *EMBO J* **23**:1657–1668.
Hediger MA, Johnson RJ, Miyazaki H, and Endou H (2005) Molecular physiology of urate transport. *Physiology (Bethesda)* **20**:125–133.
Horikawa Y, Iwasaki N, Hara M, Furuta H, Hinokio Y, Cockburn BN, Lindner T, Yamagata K, Ogata M, Tomonaga O, et al. (1997) Mutation in hepatocyte nuclear factor-1 beta gene (TCF2) associated with MODY. *Nat Genet* **17**:384–385.
Hosoyamada M, Ichida K, Enomoto A, Hosoya T, and Endou H (2004) Function and localization of urate transporter 1 in mouse kidney. *J Am Soc Nephrol* **15**:261–268.
Ichida K, Hosoyamada M, Hisatome I, Enomoto A, Hikita M, Endou H, and Hosoya T (2004) Clinical and molecular analysis of patients with renal hypouricemia in Japan-influence of URAT1 gene on urinary urate excretion. *J Am Soc Nephrol* **15**:164–173.
Imaoka T, Kusuhara H, Adachi-Akahane S, Hasegawa M, Morita N, Endou H, and Sugiyama Y (2004) The renal-specific transporter mediates facilitative transport of organic anions at the brush border membrane of mouse renal tubules. *J Am Soc Nephrol* **15**:2012–2022.
Iwai N, Mino Y, Hosoyamada M, Tago N, Kokubo Y, and Endou H (2004) A high prevalence of renal hypouricemia caused by inactive SLC22A12 in Japanese. *Kidney Int* **66**:935–944.
Kikuchi R, Kusuhara H, Hattori N, Shiota K, Kim I, Gonzalez FJ, and Sugiyama Y (2006) Regulation of the expression of human organic anion transporter 3 by hepatocyte nuclear factor 1α/β and DNA methylation. *Mol Pharmacol* **70**:887–896.
Lazzaro D, De Simone V, De Magistris L, Lehtonen E, and Cortese R (1992) LFB1 and LFB3 homeoproteins are sequentially expressed during kidney development. *Development* **114**:469–479.
Ledermann HM (1995) Is maturity onset diabetes at young age (MODY) more common in Europe than previously assumed? *Lancet* **345**:648.
Lee YH, Sauer B, and Gonzalez FJ (1998) Laron dwarfism and non-insulin-dependent diabetes mellitus in the Hnf-1alpha knockout mouse. *Mol Cell Biol* **18**:3059–3068.
Li T, Walsh JR, Ghishan FK, and Bai L (2004) Molecular cloning and characterization of a human urate transporter (hURAT1) gene promoter. *Biochim Biophys Acta* **1681**:53–58.
Magoula I, Tsapas G, Paletas K, and Mavromatidis K (1991) Insulin-dependent diabetes and renal hypouricemia. *Nephron* **59**:21–26.
Maher JM, Slitt AL, Callaghan TN, Cheng X, Cheung C, Gonzalez FJ, and Klaassen CD (2006) Alterations in transporter expression in liver, kidney, and duodenum after targeted disruption of the transcription factor HNF1alpha. *Biochem Pharmacol* **72**:512–522.
Mendel DB and Crabtree GR (1991) HNF-1, a member of a novel class of dimerizing homeodomain proteins. *J Biol Chem* **266**:677–680.
Pontoglio M, Barra J, Hadchouel M, Doyen A, Kress C, Bach JP, Babinet C, and Yaniv M (1996) Hepatocyte nuclear factor 1 inactivation results in hepatic dysfunction, phenylketonuria, and renal Fanconi syndrome. *Cell* **84**:575–585.
Pontoglio M, Prie D, Cheret C, Doyen A, Leroy C, Froguel P, Velho G, Yaniv M, and Friedlander G (2000) HNF1alpha controls renal glucose reabsorption in mouse and man. *EMBO Rep* **1**:359–365.
Pontoglio M, Sreenan S, Roe M, Pugh W, Ostrega D, Doyen A, Pick AJ, Baldwin A, Velho G, Froguel P, et al. (1998) Defective insulin secretion in hepatocyte nuclear factor 1alpha-deficient mice. *J Clin Invest* **101**:2215–2222.
Rafey MA, Lipkowitz MS, Leal-Pinto E, and Abramson RG (2003) Uric acid transport. *Curr Opin Nephrol Hypertens* **12**:511–516.
Rey-Campos J, Chouard T, Yaniv M, and Cereghini S (1991) vHNF1 is a homeoprotein that activates transcription and forms heterodimers with HNF1. *EMBO J* **10**:1445–1457.
Ryffel GU (2001) Mutations in the human genes encoding the transcription factors of the hepatocyte nuclear factor (HNF)1 and HNF4 families: functional and pathological consequences. *J Mol Endocrinol* **27**:11–29.
Shichiri M, Iwamoto H, and Shiigai T (1987) Diabetic renal hypouricemia. *Arch Intern Med* **147**:225–228.
Shih DQ, Bussen M, Sehayek E, Ananthanarayanan M, Shneider BL, Suchy FJ, Shefer S, Bollileni JS, Gonzalez FJ, Breslow JL, et al. (2001) Hepatocyte nuclear factor-1alpha is an essential regulator of bile acid and plasma cholesterol metabolism. *Nat Genet* **27**:375–382.
Shiota K (2004) DNA methylation profiles of CpG islands for cellular differentiation and development in mammals. *Cytogenet Genome Res* **105**:325–334.
Tronche F and Yaniv M (1992) HNF1, a homeoprotein member of the hepatic transcription regulatory network. *Bioessays* **14**:579–587.
Winter WE and Silverstein JH (2000) Molecular and genetic bases for maturity onset diabetes of youth. *Curr Opin Pediatr* **12**:388–393.
Yamagata K, Oda N, Kaisaki PJ, Menzel S, Furuta H, Vaxillaire M, Southam L, Cox RD, Lathrop GM, Boriraj VV, et al. (1996) Mutations in the hepatocyte nuclear factor-1alpha gene in maturity-onset diabetes of the young (MODY3). *Nature* **384**:455–458.

Address correspondence to: Dr. Yuichi Sugiyama, Department of Molecular Pharmacokinetics, Graduate School of Pharmaceutical Sciences, The University of Tokyo, 7-3-1 Hongo, Bunkyo-ku, Tokyo 113-0033, Japan. E-mail: sugiyama@mol.f.u-tokyo.ac.jp

Pharmacogenetic Characterization of Sulfasalazine Disposition Based on *NAT2* and *ABCG2* (BCRP) Gene Polymorphisms in Humans

Y Yamasaki[1], I Ieiri[1], H Kusuhara[2], T Sasaki[1], M Kimura[3], H Tabuchi[1], Y Ando[1], S Irie[3], JA Ware[4], Y Nakai[5], S Higuchi[1] and Y Sugiyama[2]

The role of breast cancer resistance protein (BCRP), an efflux ABC transporter, in the pharmacokinetics of substrate drugs in humans is unknown. We investigated the impact of genetic polymorphisms of *ABCG2* (421 C>A) and *NAT2* on the pharmacokinetics of sulfasalazine (SASP), a dual substrate, in 37 healthy volunteers, taking 2,000 mg of conventional SASP tablets. In *ABCG2*, SASP AUC_{0-48} of C/C, C/A, and A/A subjects was 171 ± 85, 330 ± 194, and 592 ± 275 μg h/ml, respectively, with significant differences among groups. In contrast, AUC_{0-48} of sulfapyridine (SP) tended to be lower in subjects with the *ABCG2-A* allele as homozygosity. In *NAT2*, AUC_{AcSP}/AUC_{SP} was significantly higher in rapid than in intermediate and slow acetylator (SA) genotypes. We successfully described the pharmacokinetics of SASP, SP, and *N*-acetylsulfapyridine (AcSP) simultaneously by nonlinear mixed-effects modeling (NONMEM) analysis with regard to both gene polymorphisms. The data indicate that SASP is a candidate probe of BCRP, particularly in its role in intestinal absorption.

INTRODUCTION

Sulfasalazine (SASP) has long been used in the treatment of inflammatory bowel diseases, such as ulcerative colitis and Crohn's disease, and rheumatoid disease.[1,2] After oral administration, SASP breaks down into sulfapyridine (SP) and 5-aminosalicylic acid (5-ASA) by bacterial azo reductases in the colon and cecum (Figure 1).[3,4] 5-ASA is suggested to be effective for inflammatory bowel diseases, while SASP and SP are effective for rheumatoid disease.[5–7] In contrast to 5-ASA, the systemic uptake of SP is virtually complete, and it is further metabolized by polymorphic *N*-acetyltransferase 2 (NAT2) into *N*-acetylsulfapyridine (AcSP) in the liver.[7–10]

The *NAT2* gene, located on chromosome 8p22, demonstrates large interindividual variability in acetylating activity by genetic polymorphism in humans.[11–15] At present, at least 35 variants have been identified,[16] and some of these mutant alleles show low acetylating activities, leading to adverse reactions of SP, such as blood disorders, including thrombocytopenia and reticulocytosis, and hepatic disorders.[17–19] *NAT2*5B*, *NAT2*6A*, and *NAT2*7B* are principally important mutant alleles, and the Japanese population can be stratified by genotyping tests into three groups: rapid acetylators (RAs), intermediate acetylators (IAs), and slow acetylators (SAs).[12–14] Low acetylating activities of SP to AcSP cause higher plasma concentrations of SP, which increase the possibility of adverse reactions in SA compared to RA; higher incidences of nausea/vomiting and hepatic disorders were reported in SA subjects.[17–19] Association between *NAT2* polymorphism (*NAT2*7B*) and Crohn's disease has also been reported in Japanese patients.[20] Although genotyping of *NAT2* provides useful information about the individual metabolic capacity of SP, the reason(s) for substantial interindividual variabilities in pharmacokinetic/pharmacodynamic profiles of SASP, a parent drug of SP, have not yet been elucidated.[10] The individual variability of bacterial azo reductase activity is speculated to affect the degradation of SASP.[3,4,17]

Breast cancer resistance protein (BCRP, *ABCG2* gene) is an efflux ABC transporter, which is expressed at the apical membrane in the placenta (trophoblast cells), liver (bile

[1]Department of Clinical Pharmacokinetics, Graduate School of Pharmaceutical Sciences, Kyushu University, Fukuoka, Japan; [2]Department of Molecular Pharmacokinetics, Graduate School of Pharmaceutical Sciences, The University of Tokyo, Tokyo, Japan; [3]Kyushu Clinical Pharmacology Research Clinic, Fukuoka, Japan; [4]Department of Pharmacokinetics, Dynamics, and Metabolism, Pfizer Global Research and Development, Michigan Labs, Ann Arbor, Michigan, USA; [5]Department of Pharmacokinetics, Dynamics, and Metabolism, Pfizer Global Research and Development, Nagoya Labs, Taketoyo, Japan.
Correspondence: Y Sugiyama (sugiyama@mol.f.u-tokyo.ac.jp)

Received 5 July 2007; accepted 25 October 2007; advance online publication 2 January 2008. doi:10.1038/sj.clpt.6100459

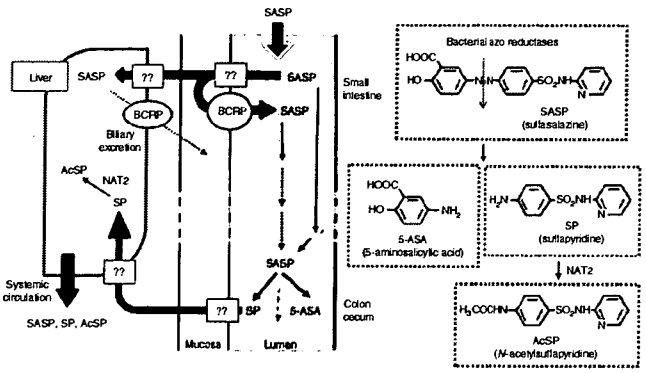

Figure 1 The possible biological fates of orally administered sulfasalazine (SASP) (in a conventional tablet form) in humans. After absorption from the luminal side, SASP is excreted into the luminal side again by breast cancer resistance protein (BCRP), which is expressed at the apical membrane of enterocytes (BCRP restricts intestinal SASP absorption). The remaining SASP travels down the small intestine to the lower intestinal tract where its diazo-bond is cleaved by colonic bacteria with the liberation of sulfapyridine (SP) and 5-aminosalicylic acid (5-ASA). SP is almost totally absorbed from the colon and cecum, and then metabolized into *N*-acetylsulfapyridine (AcSP) by *N*-acetyltransferase 2 (NAT2), predominantly in the liver.

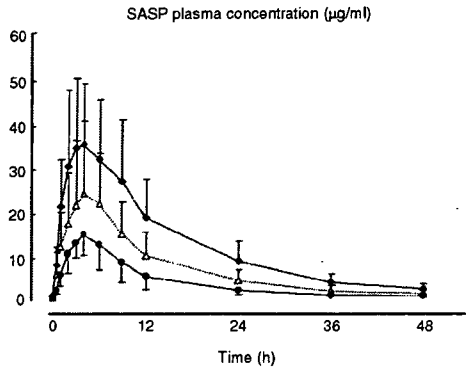

Figure 2 Effect of *ABCG2* genotype on pharmacokinetics of sulfasalazine (SASP). Plasma concentration-time profiles of SASP after oral administration of a 2,000 mg conventional SASP tablet to 421C/C subjects (closed circles, $n = 12$), 421C/A subjects (open triangles, $n = 16$), and 421A/A subjects (closed diamonds, $n = 9$).

canalicular membrane of hepatocytes), kidney, and intestine (enterocytes),[21–25] and is involved in the absorption and excretion of various drugs such as topotecan,[26] diflomotecan,[27] and rosuvastatin.[28] Recently, Zaher *et al.*[29] reported that BCRP (*ABCG2*) is an important determinant of oral bioavailability and the elimination of SASP in mice, and that SASP has the potential to be utilized as a specific *in vivo* probe of BCRP. They showed that after oral administration of SASP, the area under the plasma concentration (AUC) time profile in $BCRP^{-/-}$ mice was >100 times higher than that in **FVB** wild-type (WT) mice, and that after intravenous administration, the AUC of SASP in $BCRP^{-/-}$ mice was ~13-fold higher than that in WT mice.

Similar to the *NAT2* gene, different variants have been identified in the *ABCG2* gene. Among them, two frequent nonsynonymous variants, 34G>A (12Val>Met in exon 2) and 421C>A (141Gln>Lys in exon 5), are of interest. Pharmacokinetic profiles of topotecan,[26] diflomotecan,[27] and rosuvastatin[28] are significantly different among *ABCG2* genotyping groups. Recent clinical studies demonstrated that *ABCG2* 421C>A polymorphism was associated with gefitinib accumulation at steady state,[30] leading to an increased risk of diarrhea.[31] In contrast to these drugs, however, no remarkable change in pitavastatin pharmacokinetics has recently been reported,[32] suggesting that the effect of the *ABCG2* polymorphism underlies the substrate-dependent activity.

In this study, we demonstrate the synchronized contribution of drug transporter and metabolism gene polymorphisms to the pharmacokinetics of SASP in healthy subjects, who were selected from our study panels based on their genotypes of *ABCG2* (421C>A) and *NAT2* (*NAT2*4*, *5B, *6A, and *7B).

RESULTS

No clinically undesirable signs and symptoms possibly attributed to the administration of SASP were recognized throughout the study. All subjects completed the study successfully according to the protocol.

SASP pharmacokinetics in relation to *ABCG2* and *NAT2* genotypic status

After oral administration, the mean plasma concentrations of SASP were significantly higher ($P < 0.01$) in *ABCG2-A/A* subjects than in *ABCG2-C/C* subjects, and *ABCG2-C/A* subjects had values between those in *ABCG2-A/A* and *ABCG2-C/C* subjects at all observation points except 0.5 h (Figure 2). The mean (± SD) AUC_{0-48} of SASP in *ABCG2-C/C* ($n = 12$), *ABCG2-C/A* ($n = 16$), and *ABCG2-A/A* ($n = 9$) subjects was 171 ± 85, 330 ± 194, and 592 ± 275 μg h/ml, respectively, and significant differences ($P < 0.05$) were observed among all three groups (Table 1). Similarly, the mean peak plasma concentration (Cmax) in *ABCG2-C/C*, *ABCG2-C/A*, and *ABCG2-A/A* subjects was 15.4 ± 5.2, 26.4 ± 16.1, and 40.7 ± 13.5 μg/ml, respectively, with significant differences among all three groups. In contrast, the mean CL_{total}/F in *ABCG2-C/C*, *ABCG2-C/A*, and *ABCG2-A/A* subjects was 13.7 ± 5.8, 7.3 ± 3.0, and 3.7 ± 1.3 l/h, respectively.

For combined *ABCG2* and *NAT2* genotypes, the number of patients within each combination of genotypes and pharmacokinetic parameters are summarized in Table 2. The mean AUC_{0-48} of SASP in groups RA-C/C, C/A, and A/A was 146 ± 43, 282 ± 78, and 742 ± 469, and in groups IA-C/C, C/A, and A/A was 171 ± 80, 310 ± 151, and 517 ± 113 μg h/ml, respectively; the mean value in *ABCG2-A/A* subjects was significantly higher than that in subjects C/A and C/C in both RA and IA. A similar trend was observed in C_{max} values. In contrast, mean CL_{total}/F in groups RA-C/C, C/A, and A/A was 14.4 ± 4.5, 7.3 ± 2.1, and 3.3 ± 1.9, and in groups IA-C/C, C/A, and A/A was 13.6 ± 6.8, 7.6 ± 3.8, and 3.9 ± 1.0 l/h, respectively; the mean value in *ABCG2-A/A* subjects was significantly lower than that in C/C subjects in both RA and IA.

The mean AUC_{0-48} of SASP in groups RA-C/C, IA-C/C, and SA-C/C was 146 ± 43, 171 ± 80, and 237, and in groups RA-C/A, IA-C/A, and SA-C/A was 282 ± 78, 310 ± 151, and 387 ± 289 μg h/ml, respectively; no significant intergenotypic

Table 1 Pharmacokinetic parameters of SASP after single oral dose of SASP with regard to the polymorphism of *ABCG2* gene

Genotype *ABCG2*	*n*	AUC_{0-48} (μg h/ml)	K_e (h^{-1})	CL_{total}/F (l/h)	$t_{1/2}$ (h)	T_{max} (h)	C_{max} (μg/ml)
C/C	12	171 ± 85 (123 ~ 220)	0.08 ± 0.03 (0.07 ~ 0.10)	13.7 ± 5.8 (10.4 ~ 16.9)	9.8 ± 4.5 (7.2 ~ 12.3)	4.3 ± 0.9 (3.8 ~ 4.7)	15.4 ± 5.2 (12.4 ~ 18.4)
C/A	16	330 ± 194* (235 ~ 425)	0.07 ± 0.01 (0.06 ~ 0.07)	7.3 ± 3.0* (5.8 ~ 8.8)	10.5 ± 2.0 (9.5 ~ 11.5)	4.8 ± 1.6 (4.1 ~ 5.6)	26.4 ± 16.1* (18.5 ~ 34.3)
A/A	9	592 ± 275*,** (412 ~ 771)	0.07 ± 0.01 (0.06 ~ 0.07)	3.7 ± 1.3*,** (2.9 ~ 4.6)	10.3 ± 1.5 (9.4 ~ 11.3)	3.9 ± 2.2 (2.5 ~ 5.3)	40.7 ± 13.5*,** (31.8 ~ 49.5)

Each value represents the mean ± SD (95% confidence interval).

SASP, sulfasalazine (salazosulfapyridine).

*Significantly different from values in C/C subjects as determined by ANOVA with Fisher's least significant difference test ($P < 0.05$). **Significantly different from values in C/A subjects as determined by ANOVA with Fisher's least significant difference test ($P < 0.05$).

Table 2 Pharmacokinetic parameters of SASP after single oral dose of SASP with regard to the polymorphism of *ABCG2* and *NAT2* genes

Genotype *NAT2*	*ABCG2*	*n*	AUC_{0-48} (μg h/ml)	K_e (h^{-1})	CL_{total}/F (l/h)	$t_{1/2}$ (h)	T_{max} (h)	C_{max} (μg/ml)
RA	C/C	5	146 ± 43 (108 ~ 183)	0.08 ± 0.02 (0.06 ~ 0.10)	14.4 ± 4.5 (10.5 ~ 18.3)	9.8 ± 4.3 (6.0 ~ 13.5)	3.8 ± 0.5 (3.4 ~ 4.2)	13.6 ± 2.6 (11.3 ~ 15.9)
	C/A	5	282 ± 78 (215 ~ 350)	0.07 ± 0.01 (0.06 ~ 0.08)	7.3 ± 2.1* (5.4 ~ 9.2)	10.5 ± 2.3 (8.5 ~ 12.4)	4.4 ± 1.5 (3.1 ~ 5.7)	23.4 ± 8.3 (16.1 ~ 30.7)
	A/A	3	742 ± 469*,** (212 ~ 1272)	0.07 ± 0.01 (0.06 ~ 0.08)	3.3 ± 1.9* (1.2 ~ 5.5)	10.4 ± 1.1 (9.1 ~ 11.6)	4.7 ± 3.8 (0.4 ~ 9.0)	44.4 ± 24.5*,** (16.7 ~ 72)
IA	C/C	5	171 ± 80 (101 ~ 241)	0.08 ± 0.03 (0.06 ~ 0.11)	13.6 ± 6.8 (7.6 ~ 19.5)	10.0 ± 5.9 (4.8 ~ 15.3)	4.4 ± 0.9 (3.6 ~ 5.2)	15.9 ± 6.4 (10.2 ~ 21.5)
	C/A	5	310 ± 151 (178 ~ 442)	0.07 ± 0.01 (0.06 ~ 0.07)	7.6 ± 3.8 (4.3 ~ 10.9)	10.5 ± 1.1 (9.5 ~ 11.5)	4.6 ± 1.3 (3.4 ~ 5.8)	22.6 ± 10.7 (13.2 ~ 32.0)
	A/A	6	517 ± 113*,** (426 ~ 607)	0.07 ± 0.01 (0.06 ~ 0.08)	3.9 ± 1.0* (3.1 ~ 4.7)	10.3 ± 1.7 (8.9 ~ 11.7)	3.2 ± 1.3 (2.1 ~ 4.2)	38.8 ± 6.3*,** (33.7 ~ 43.9)
SA	C/C	2	237	0.08	12	9.1	5	18.7
	C/A	6	387 ± 289 (156 ~ 618)	0.07 ± 0.01 (0.06 ~ 0.08)	6.9 ± 3.5 (4.1 ~ 9.8)	10.5 ± 2.5 (8.5 ~ 12.6)	4.8 ± 2.0 (3.2 ~ 6.5)	31.1 ± 24.0 (12.0 ~ 50.3)

Each value represents the mean ± SD (95% confidence interval).

IA, intermediate acetylator [*4/*6A ($n = 10$), *4/*7B ($n = 6$)]; RA, rapid acetylator (*4/*4); SA, slow acetylator [*6A/*6A ($n = 4$), *6A/*7B ($n = 4$)]; SASP, sulfasalazine (salazosulfapyridine).

*Significantly different from values in C/C subjects within the same NAT2 genotyping group as determined by ANOVA with Fisher's least significant difference test ($P < 0.05$).
**Significantly different from values in C/A subjects within the same NAT2 genotyping group as determined by ANOVA with Fisher's least significant difference test ($P < 0.05$).

difference was observed. Similar trends were observed in mean CL_{total}/F and C_{max} values, suggesting that *NAT2* polymorphism is not a determinant of the pharmacokinetics of SASP.

No intergenotypic differences were observed in mean elimination rate constant (K_e) and time to reach the maximum concentration (T_{max}) values.

SP and AcSP pharmacokinetics in relation to *ABCG2* and *NAT2* genotypic status

Pharmacokinetic parameters of SP after a single oral dose of SASP are summarized in Table 3. In contrast to SASP, the mean AUC_{0-48} of SP tended to be lower in *ABCG2-A/A* subjects; the order was *ABCG2-C/C* > C/A > A/A in both RA and IA types of the *NAT2* gene. A similar trend was observed in C_{max} values. The mean AUC_{0-48}, $t_{1/2}$, and C_{max} values of SP were significantly different among three *ABCG2-C/A* matched *NAT2* genotyping subjects; the order was SA > IA > RA, suggesting that pharmacokinetic profiles of SP depend both on *NAT2* and *ABCG2* polymorphisms.

Although the mean AUC_{0-48} and C_{max} of AcSP tended to be lower in *ABCG2-A/A* subjects, there were no significant differences in any of the pharmacokinetics parameters of AcSP among all *ABCG2* genotyping groups (Table 4).

With regard to the *NAT2* polymorphism alone, the mean AUC ratio of AcSP to SP (AUC_{AcSP}/AUC_{SP}) in RA, IA, and SA subjects was 3.1 ± 0.6, 1.9 ± 0.5, and 0.5 ± 0.4, respectively, with significant differences among all groups; however, the mean renal clearance (CL_r) value was comparable among all groups for both SP and AcSP (Table 5).

Simultaneous modeling and NONMEM analysis of SASP, SP, and AcSP in relation to *ABCG2* and *NAT2* polymorphisms

There were significant correlations between individual post-hoc prediction values and observed values (i.e., actual plasma

Table 3 Pharmacokinetic parameters of SP after single oral dose of SASP with regard to the polymorphism of *ABCG2* and *NAT2* genes

Genotype							
NAT2	*ABCG2*	*n*	AUC_{0-48} (μg h/ml)	K_e (h^{-1})	$t_{1/2}$ (h)	T_{max} (h)	C_{max} (μg/ml)
RA	C/C	5	140 ± 35 (109 ~ 171)	0.10 ± 0.01 (0.09 ~ 0.11)	7.2 ± 0.8 (6.5 ~ 7.9)	10.8 ± 2.7 (8.5 ~ 13.2)	6.3 ± 1.1 (5.3 ~ 7.3)
	C/A	5	134 ± 32* (106 ~ 162)	0.10 ± 0.02* (0.07 ~ 0.11)	7.9 ± 2.0* (6.2 ~ 9.7)	13.8 ± 5.8 (8.7 ~ 18.9)	5.7 ± 1.1* (4.7 ~ 6.6)
	A/A	3	84 ± 28 (53 ~ 116)	0.08 ± 0.03 (0.05 ~ 0.11)	9.2 ± 2.8 (6.1 ~ 12.3)	20.0 ± 6.9 (12.2 ~ 27.8)	3.7 ± 1.3**,*** (2.2 ~ 5.2)
IA	C/C	5	189 ± 55 (140 ~ 237)	0.06 ± 0.03 (0.04 ~ 0.09)	12.6 ± 5.0 (8.2 ~ 16.9)	21.6 ± 10 (12.8 ~ 30.4)	7.7 ± 3.1 (5.0 ~ 10.4)
	C/A	5	171 ± 82* (99 ~ 243)	0.08 ± 0.02* (0.06 ~ 0.09)	9.4 ± 1.6* (8.0 ~ 10.8)	13.8 ± 5.8 (8.7 ~ 18.9)	7.5 ± 3.5* (4.4 ~ 10.5)
	A/A	6	140 ± 58 (93 ~ 187)	0.07 ± 0.03 (0.04 ~ 0.09)	12.5 ± 6.0 (7.7 ~ 17.3)	18.0 ± 6.6 (12.7 ~ 23.3)	5.6 ± 2.3 (3.8 ~ 7.5)
SA	C/C	2	170	0.07	10.1	12.0	6.6
	C/A	6	357 ± 99 (278 ~ 437)	0.04 ± 0.02 (0.03 ~ 0.05)	19.4 ± 7.5 (13.4 ~ 25.4)	20.0 ± 6.2 (15.0 ~ 25.0)	12.7 ± 2.5 (10.7 ~ 14.7)

Each value represents the mean ± SD (95% confidence interval).

IA, intermediate acetylator [*4/*6A ($n = 10$), *4/*7B ($n = 6$)]; RA, rapid acetylator (*4/*4); SA, slow acetylator [*6A/*6A ($n = 4$), *6A/*7B ($n = 4$)]; SASP, sulfasalazine (salazosulfapyridine); SP, sulfapyridine.

*Significantly different from values in *SA-ABCG2-C/A* subjects as determined by ANOVA with Fisher's least significant difference test ($P < 0.05$). **Significantly different from values in C/A subjects within the same *NAT2* genotyping group as determined by ANOVA with Fisher's least significant difference test ($P < 0.05$). ***Significantly different from values in C/C subjects within the same *NAT2* genotyping group as determined by ANOVA with Fisher's least significant difference test ($P < 0.05$).

Table 4 Pharmacokinetic parameters of AcSP after single oral dose of SASP with regard to the polymorphism of *ABCG2* and *NAT2* genes

Genotype							
NAT2	*ABCG2*	*n*	AUC_{0-48} (μg h/ml)	K_e (h^{-1})	$t_{1/2}$ (h)	T_{max} (h)	C_{max} (μg/ml)
RA	C/C	5	425 ± 148 (295 ~ 555)	0.09 ± 0.02 (0.07 ~ 0.10)	8.2 ± 1.8 (6.6 ~ 9.9)	24.0	16.3 ± 5.4 (11.5 ~ 21.1)
	C/A	5	445 ± 139*,** (324 ~ 566)	0.07 ± 0.02* (0.06 ~ 0.09)	10.2 ± 3.1* (7.5 ~ 13.0)	21.6 ± 5.4 (16.9 ~ 26.3)	17.6 ± 5.1*,** (13.2 ~ 22.1)
	A/A	3	250 ± 42 (202 ~ 298)	0.06 ± 0.04 (0.01 ~ 0.10)	15.9 ± 8.3 (6.5 ~ 25.3)	24.0	9.8 ± 1.8 (7.7 ~ 11.8)
IA	C/C	5	345 ± 146 (217 ~ 473)	0.05 ± 0.03 (0.02 ~ 0.08)	23.2 ± 21.0 (4.8 ~ 41.6)	28.8 ± 6.6 (23.0 ~ 34.6)	12.6 ± 5.2 (8.0 ~ 17.2)
	C/A	5	281 ± 129 (168 ~ 393)	0.06 ± 0.01* (0.05 ~ 0.07)	12.0 ± 2.4* (9.9 ~ 14.1)	21.6 ± 5.4 (16.9 ~ 26.3)	10.5 ± 4.6* (6.5 ~ 14.5)
	A/A	6	270 ± 109 (182 ~ 357)	0.05 ± 0.03 (0.03 ~ 0.08)	19.3 ± 12.8 (9.0 ~ 29.5)	24.0 ± 7.6 (17.9 ~ 30.1)	9.3 ± 3.4 (6.6 ~ 12.0)
SA	C/C	2	48.0	0.1	8.7	24.0	2.1
	C/A	6	146 ± 45 (110 ~ 182)	0.02 ± 0.01 (0.01 ~ 0.03)	50.1 ± 34.2 (22.2 ~ 77.5)	26.0 ± 4.9 (22.1 ~ 29.9)	5.1 ± 1.7 (3.7 ~ 6.4)

Each value represents the mean ± SD (95% confidence interval).

AcSP, *N*-acetylsulfapyridine; SASP, sulfasalazine (salazosulfapyridine).

*Significantly different from values in *SA-ABCG2-C/A* subjects as determined by ANOVA with Fisher's least significant difference test ($P < 0.05$). **Significantly different from values in *IA-ABCG2-C/A* subjects as determined by ANOVA with Fisher's least significant difference test ($P < 0.05$).

Table 5 Pharmacokinetic parameters of SP and AcSP after single oral dose of SASP in three *NAT2* genotyping groups

			SP		AcSP	
Genotype	*n*	AUC_{AcSP}/AUC_{SP}	CL_r (l/h)	48-h Cumulative urinary excretion (%)	CL_r (l/h)	48-h Cumulative urinary excretion (%)
RA	13	3.1 ± 0.6 (2.8 ~ 3.5)	0.52 ± 0.09 (0.47 ~ 0.57)	5.2 ± 2.0 (4.2 ~ 6.3)	1.6 ± 0.3 (1.4 ~ 1.8)	41.5 ± 12.5 (34.7 ~ 48.3)
IA	16	1.9 ± 0.5* (1.7 ~ 2.1)	0.55 ± 0.07 (0.52 ~ 0.59)	7.3 ± 3.1 (5.8 ~ 8.8)	1.9 ± 0.4 (1.7 ~ 2.0)	36.7 ± 13.6 (30.0 ~ 43.3)
SA	8	0.5 ± 0.4*,** (0.3 ~ 0.8)	0.50 ± 0.06 (0.46 ~ 0.54)	12.7 ± 6.3*,** (8.3 ~ 17.1)	2.0 ± 0.6 (1.6 ~ 2.4)	15.9 ± 6.8*,** (11.2 ~ 20.6)

Each value represents the mean ± SD (95% confidence interval).

AcSP, *N*-acetylsulfapyridine; CLr, renal clearance; IA, intermediate acetylator; RA, rapid acetylator; SA, slow acetylator; SASP, sulfasalazine (salazosulfapyridine); SP, sulfapyridine.

*Significantly different from values in RA subjects as determined by ANOVA with Fisher's least significant difference test ($P < 0.001$). **Significantly different from values in IA subjects as determined by ANOVA with Fisher's least significant difference test ($P < 0.001$).

concentrations) for SASP, SP, and AcSP (Figure 3). Individual fitting curves of the three compounds in typical subjects are presented in Figure 4. Nonlinear mixed-effects modeling (NONMEM) analysis confirmed that individual *ABCG2* and *NAT2* genotyping status was a statistically significant predictor of SASP, and SP and AcSP pharmacokinetics, respectively (Figures 3 and 4, Table 6). Incorporating the effect of *ABCG2* genotype on SASP relative bioavailability (Fr, assumed 1.0 for *ABCG2-C/C* subjects), Ka, and CL/F (CL_{SASP}/F), and of *NAT2* genotype on CL_{SP} (formation CL of AcSP) was associated with significant

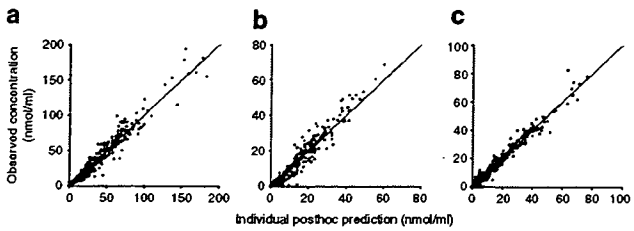

Figure 3 Scatter plots of observed plasma concentrations vs. individual posthoc prediction values of (**a**) sulfasalazine, (**b**) sulfapyridine, and (**c**) *N*-acetylsulfapyridine. The solid line is the line of identity.

Table 6 Population pharmacokinetic parameters and their variabilities for SASP, SP, and AcSP in basic and final models estimated by NONMEM with regard to *ABCG2* and *NAT2* gene polymorphisms

		Population mean (SE) (95%, confidence interval)		Variability (CV% (SE))	
Parameter/effect		Basic model	Final model	Basic model	Final model
SASP	K_a (h^{-1})	0.62 (0.16)	0.42 (0.08)	40.7 (25.1)	42.7 (26.5)
	CL/F (l/h)	5.3 (0.87)	9.3 (1.7)	125 (92.6)	111 (71.1)
	V_c/F (l)	47.8 (8.3)	74.4 (12.3)	55.7 (35.3)	50.5 (30.1)
	Q/F (l/h)	1.1 (0.36)	1.9 (0.43)	0 Fixed (–)	0 Fixed (–)
	V_p/F (l)	62.0 (28.3)	159 (67.3)	125 (78.4)	150 (95.2)
	Tlag (h)	0.25 (0.05)	0.25 (0.05)	42.8 (42.1)	68.5 (73.3)
SP	K_{TR} (h^{-1})	0.31 (0.05)	0.32 (0.02)	34.5 (19.4)	28.5 (16.0)
	CL_{SP} (l/h)	1.6 (0.36)	3.6 (0.49)	52.6 (31.0)	9.5 (8.4)
	V_{SP} (l/h)	26.7 (5.9)	32.7 (4.9)	41.3 (28.6)	70.9 (43.0)
AcSP	CL_{AcSP} (l/h)	1.3 (0.33)	1.3 (0.19)	72.6 (50.9)	3.0 (9.9)
	V_{AcSP} (l)	7.4 (2.8)	6.3 (1.0)	46.1 (31.0)	19.3 (12.0)
Genotyping effect					
	CL_{SP} (IA)	–	0.69 (0.04) [0.61–0.77]		
	CL_{SP} (SA)	–	0.18 (0.03) [0.12–0.24]		
	Fr (C/A)	–	1.7 (0.25) [1.2–2.2]		
	Fr (A/A)	–	2.1 (0.41) [1.3–3.0]		
	K_a (A/A)	–	1.8 (0.32) [1.2–2.4]		
	CL_{SASP}/F (C/A and A/A)	–	0.84 (0.02) [0.79–0.89]		
	OFV	4,168.282	3,771.129		

ABCG2 genotype effect was described as the following function: $P = P_{wildtype} \times \theta^{421C/A} \times \theta^{421A/A}$. NAT2 genotype effect was described as the following function: $P = P_{RA} \times \theta^{IA} \times \theta^{SA}$.

A/A, *ABCG2-A/A*; AcSP, *N*-acetylsulfapyridine; C/A, *ABCG2-C/A*; CL/F, apparent clearance; CL_{AcSP}, clearance of AcSP; CL_{SP}, formation clearance to AcSP; IA, intermediate acetylator; K_a, absorption rate constant; K_{TR}, transfer rate constant for Erlang's distribution; NONMEM, nonlinear mixed-effects modeling; OFV, objective function value estimated by NONMEM; Q/F, intercompartment clearance; SA, slow acetylator; SASP, sulfasalazine; SP, sulfapyridine; Tlag, absorption lag time; V_{AcSP}, volume of distribution of AcSP; Vc/F, volume of distribution of central compartment; Vp/F, volume of distribution of peripheral compartment; V_{SP}, volume of distribution of SP.

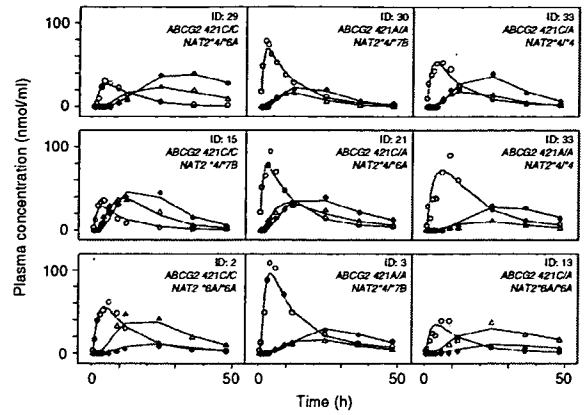

Figure 4 Observed plasma concentrations and post-hoc prediction curves in typical subjects with their *NAT2* and *ABCG2* genotyping results: sulfasalazine (open circles), sulfapyridine (open triangles), and *N*-acetylsulfapyridine (closed diamonds).

reduction in the objective function value (4,168.282→3,771.129). SASP Fr and Ka were increased, and CL_{SASP}/F was decreased in subjects with the *ABCG2-A* allele(s); the relative value of Fr in *ABCG2-C/C*, C/A, and A/A subjects was 1:1.7:2.1. The relative Ka and CL_{SASP}/F values in *ABCG2-C/C*, C/A, and A/A subjects were 1:1:1.8 and 1:0.84:0.84, respectively. CL_{SP} values were lower in IA and SA subjects than in RA subjects; the relative value of CL_{SP} in RA, IA, and SA was 1:0.7:0.18. No confidence intervals were >1.0, indicating that the contribution of the genotype to each parameter was significant. In **PPK** analysis, we fixed the interindividual variability of Q/F to zero; however, this treatment did not interfere with predictive performance (data not shown).

DISCUSSION

The aim of this study was to evaluate whether the polymorphism of drug metabolism and transporter genes is simultaneously involved in the overall pharmacokinetic profile of SASP in humans. The important findings were that: (1) significant differences in AUC of SASP were observed among subjects with different *ABCG2* genotypes; (2) AUC of SP tended to be lower in *ABCG2-A/A* subjects except for SA; (3) As with previous studies, significant differences in AUC_{AcSP}/AUC_{SP} were observed among subjects with different *NAT2* genotypes; (4) NONMEM analysis also supported the contribution of both gene polymorphisms to the pharmacokinetics of SASP, SP, and AcSP.

In this study, we demonstrated that BCRP plays an important role in the pharmacokinetics of SASP in humans. After oral administration, the mean AUC_{0-48} and C_{max} of SASP were significantly higher, and the mean CL_{total}/F was significantly lower in subjects with at least one *ABCG2-A* mutant allele (Table 1). Similar results were observed when we considered the combination of *ABCG2* and *NAT2* genotyping results, suggesting that NAT2 is not involved in the pharmacokinetics of SASP (Table 2). Previous *in vivo* studies demonstrated that *ABCG2* 421C>A polymorphism was associated with changes in the pharmacokinetics of certain clinically important drugs, such as topotecan,[26]